Intercellular Communication Between Bone Cells Induced By Mechanical Stimulation

Shu Xing

Master of Science

Department of Physics

McGill University

Montreal,Quebec

2012-08

Thesis submitted to the Faculty of Graduate Studies and Research in partial fulfillment of the requirements for the degree of Master of Science

DEDICATION

To my parents who have always loved me,

to my supervisors Dr. Peter Grütter and Dr. Svetlana Komarova who treated me like family,

to all the wonderful people in my group,

and to you who are spending your time reading my work.

ACKNOWLEDGEMENTS

I would like to thank my parents to their love and support. They have always believed in me and my dreams. I wish to acknowledge my co-supervisors, Dr.Peter Grütter, for giving me an opportunity to work with AFM and all his inspiration and advice, Dr.Svetlana Komarova, for all her guidance and care in my research career ever since I was a sophomore student. Also,I would like to thank everyone in my research group, especially to Monserratt Lopez, Dr. Gulzhakhan Sadvakassova, Dr.Yoichi Miyahara for all their help. A very special thanks goes to Victor Yu for spending much time reading and correcting my thesis. For financial support, I would like to acknowledge McGill University, the Physics Department, my supervisors Dr. Grütter and Dr.Komarova for funding my studies. Finally, A big thanks to all my friends and colleagues who make me feel like home in Montreal. I love you all.

ABSTRACT

Mechanical loading is crucial in modulating the physiology and architecture of bone. Previous experiments indicated intercellular communication among osteoblasts upon mechanical stimulation, suggesting the involvement of a soluble signal mediator. Extracellular adenosine triphosphate (ATP) functions as signaling molecules in many cell regulation processes, therefore appears to be a prone candidate. ATP acts on osteoblasts through multiple P2 receptors. To provide insights on the roles of individual receptors, we modeled ATP concentration dependence for different P2 receptors. Next, the process of ATP degradation and the diffusion of ATP, adenosine diphosphate (ADP) and adenosine monophosphate (AMP) are modeled. To confirm the predictions of the model, we initiated experiments to measure ATP release from mechanically stimulated osteoblasts. Firefly luciferase assay successfully measures ATP using a luminometer and a charge coupled device (CCD) camera. Local indentation with a AFM cantilever is applied to mechanically stimulate an osteoblast. Preliminary results on real time imaging of ATP release from osteoblasts are reported.

ABRÉGÉ

Le chargement mécanique est crucial dans la modulation de la physiologie et de l'architecture de l'os. Des expériences antérieures ont indiqué la communication intercellulaire entre les ostéoblastes lors de la stimulation mécanique. Ces résultats suggèrent l'implication d'un médiateur soluble. L'adénosine triphosphate (ATP) extracellulaire fonctionne comme des molécules de signalisation dans de nombreux processus de régulation cellulaire. Celle-ci semble être un candidat à risque. L'ATP agit sur les ostéoblastes via les récepteurs P2. Ici, la concentration d'ATP pour chacun de ces récepteurs P2 a été modélisée mathématiquement pour mieux comprendre leur rôle. Le processus de dégradation de l'ATP et la diffusion de l'ATP, adénosine diphosphate (ADP) et adénosine monophosphate (AMP) ont aussi été modélisés. Avec le luminomètre, nous étions capables de mesurer avec succès l'ATP par dosage de la luciférase de luciole. Des images de haute résolution de la détection d'ATP ont été obtenues avec un dispositif à transfert de charge (CCD). Enfin, l'indentification locale avec une pointe de microscopie à force atomique (MFA) est appliquée mcaniquement pour stimuler un ostoblaste. Les rsultats préliminaires sur l'imagerie en temps réel de la libération d'ATP à partir d'ostéoblastes sont présentés.

TABLE OF CONTENTS

LIST OF TABLES

LIST OF FIGURES

CHAPTER 1
Introduction and Background

The adult human skeleton has a total of 213 bones, composed mainly of cellular and mineral components [7]. Each bone constantly undergoes modeling to adapt to the changes of environment, as well as remodeling to replace the old and damaged bones with new ones [8]. Healthy bone mass is maintained by balancing the increase of bone mass with bone loss. Excessive bone loss during aging can lead to osteoporosis, a disease characterized by low bone mass and microarchitectural deterioration of bone tissue, leading to enhanced bone fragility and a consequent increase in fracture risk [9].

Osteoporosis is also often found in young astronauts who have spent long period of time in outer space. It has been shown that micro-gravity, which astronauts experience during their journeys to outer space, leads to significant increase in bone loss [10]. The mechanism that leads to bone loss is not well understood. However, studies have suggested that portions of the human skeleton are subjected to large but transient mechanical loads during daily activities such as walking and lifting. The dynamic gravitational loading during walking and lifting is important to normal growth and maintenance of the skeleton. Under weightless conditions during space flight, the skeleton is experiencing resting loads, which could affect the bone turnover

[11]. Therefore, mechanical loading is crucial in modulating the physiology and architecture of bone tissue.

1.1 Bone cells physiology

On a cellular level, there are three types of bone cells, osteoblasts, osteoclasts and osteocytes. Osteoblasts are bone forming cells and osteoclasts are responsible for bone resorption. Osteocytes reside in the bone tissue and are believed to form a signaling network within bone.

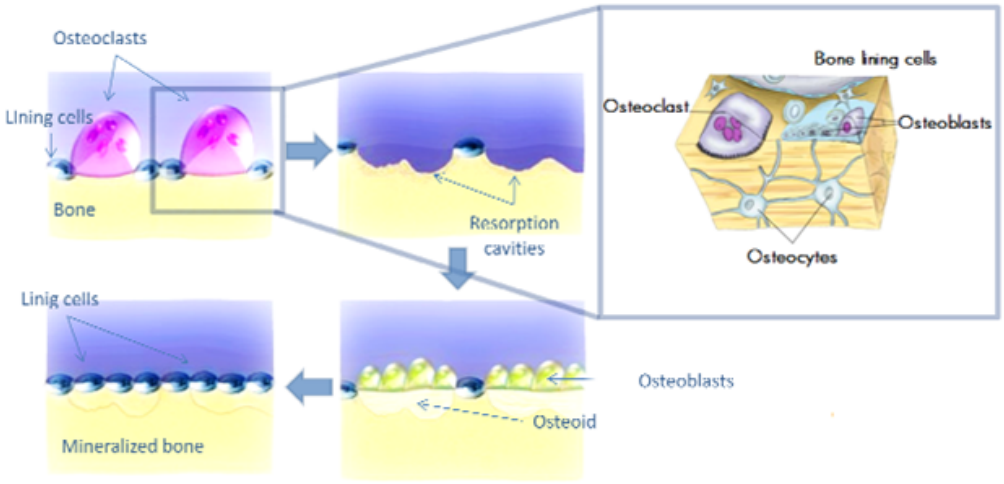

Figure 1–1: Bone cells function and remodeling [1].

During the bone remodeling process by which bone is renewed to maintain bone strength and mineral homeostasis, the mononuclear osteoclast precursors are activated. Multiple precursor cells fuse to become a multinucleated osteoclast. Next, the osteoclast binds to bone matrix proteins, forming a sealed zone around the bone

tissue. Once the process is accomplished, the osteoclast starts to secrete H^+ ions into the sealed zone, to dissolve the mineral and proteases to break down organic component of bone tissue. In order to replace the resorbed bone tissues, osteoblasts, bone formation cells, are recruited to the resorption sites. Osteoblasts synthesize new collagenous organic osteoid matrix and regulate mineralization of matrix by releasing small, membrane-bound matrix vesicles. Over time, the osteoid matrix mineralizes to become bone. The osteoblasts surrounded by and buried within this matrix become osteocytes. Osteocytes form a network within the bone to connect to the bone surface lining cells, osteoblasts and other osteocytes. The main function of osteocytes is to sense and react to mechanical strains. [8] [1]

1.2 Mechanical loading

Several models have been developed to understand the effects of mechanical stimulation on cells in vitro. Early effort in the field of cell culture mechanostimulus were of non-quantitative nature. Pioneering work was performed by Glucksmann in 1939, who grew cell culture on substrates of explanted intercostal muscle to which pairs of neighboring ribs were left attached. Over periods of several days, the cell cultures were compressed when the ribs were drawn towards one another as the muscle tissue degenerated [12]. The landmark of mechanical stimulation was the work of Rodan in 1976, when he measured the effect of compression of chick embryo cells using hydrostatic pressurization [13]. Hydrostatic pressurization holds substantial attractions, such as simplicity of the equipment and the spatial homogeneity of the stimulus [14]. However, one major limitation of this technique is the difficulty in

controlling the pressure of the gas mixture in the equipment to create a physiological environment for the cells [15]. Not long after, the longitudinal substrate stretch system was developed. This loading systems utilize a controlled uniaxial distention of deformable substrates [14]. Leung and colleagues demonstrated the changes in protein and DNA synthesis by aortic smooth muscle cells seeded on the elastin substrates [16]. The longitudinal stretch system was soon developed and extended into many techniques, including substrate bending [17], circular substrate distention [18] and in-plane substrate distention [19]. Unfortunately, these systems' applicability is limited because they utilize direct clamping of cell sheets grown previously in non-loaded culture. The removal of the culture sheet from its initial growth flask to the deformable substrate has obvious potential for confounding mechanical effects due to the transfer process itself [14].

Another approach of mechanical stimulation on cell cultures is the application of fluid shear stress. The cone-and-plate system and the parallel plate system are the two configurations which are widely used. The cone-and-plate system employs a cone of small angle, perpendicular to the surface of a flat plate. Since the torque required to rotate the cone in a fluid is a function of the viscosity of the fluid, the shear speed can be controlled by adjusting the torque [20]. A more popular configuration is the parallel plate flow chamber, in which a pressure differential is created between both sides, causing uniform laminar flow to develop across the culture surface [21].

Recently, local indentation techniques have been developed to allow the characterization of the response to mechanical stimulation at the single cell level. Studies have reported the use of pipette microinjection [22], pipette suction [23], and atomic

force microscopy (AFM) to investigate the responses of individual cells to mechanical stimulation [24] [25]. However, the first two methods can not compete with the precision that can be achieved with AFM [26]. Modern AFM techniques grant precise control over the application of force, and allow monitoring of the level of cell membrane deformation. The AFM cantilever serves as a microindenter to probe the cell, allowing the evaluation of local mechanical properties and the topography of the living cells at a high spatial resolution [27]. Moreover, different stiffness and geometries of the cantilever can provide additional control of the distribution of the force. Due to these advantages of AFM, the local indentation experiments in the last chapter of this thesis with osteoblasts will be performed with AFM.

1.3 Osteoblasts cellular responses to mechanical stimulation

Stimulation of Ca^{2+} signaling was shown to be the first response of osteoblastic cells to any type of mechanical stimulation [28] [29]. In our group, we have shown that mechanical stimulation of an osteoblast induces an increase in cytosolic free Ca^{2+} ($[Ca^{2+}]_i$) level.

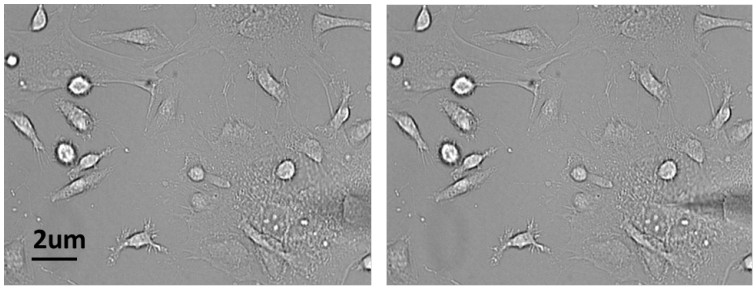

(a)

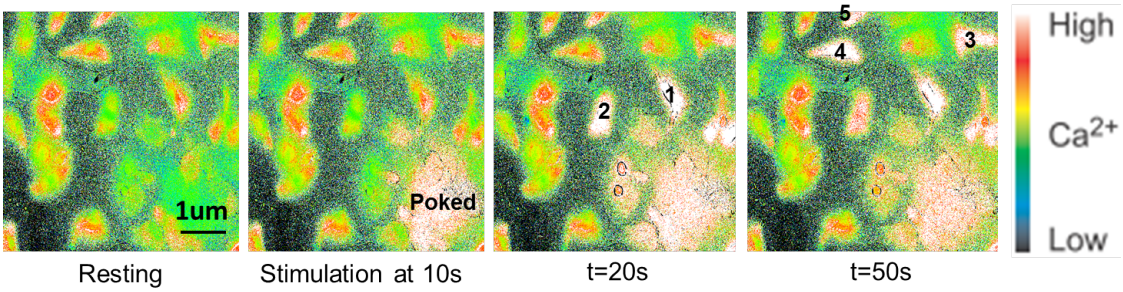

(b)

Figure 1–2: These figures are taken from Osama Maria's Thesis [2].(a) Bright field images are showing mechanical stimulation of a single bone cell by a micropipette. (b) Fluorescent images taken at indicated time demonstrate mechanical stimulation of a cell(poked) and subsequent increase in calcium in neighboring non-connected cells, indicated by numbers.

Figure 1–2 illustrates the work done by Osama Maria [2]. The bright field image shows that the injury of a single bone cell was induced by mechanical stimulation with a micropipette at 10 s. Changes in Ca^{2+} level were then examined using fluorescence microscopy of fura-2 loaded cells. Fura-2 is a fluorescent dye which emits

light upon binding to free intracellular calcium, when excited with 340 nm light [30]. Figure 1–2(b) demonstrates a series of images taken at different time. The red-white pseudocolor characterizes cells that exhibit high level of calcium. It was found that mechanical simulation of an osteoblast induces an increase in its calcium level. Moreover, there are also delayed transient elevation of calcium in five neighboring non-connected cells noticeable at t = 10 s and t = 40 s. These delayed elevations of calcium are reffered to the secondary responses. The secondary response upon mechanical stimulation indicates that osteoblasts communicate with each other, suggesting the involvement of a soluble signaling mediator.

1.4 Signal Mediators

Extracellular nucleotides were previously implicated in cell responses to mechanical forces [31]. Among the extracellular nucleotides, Adenosine Triphosphate (ATP) is found in all animal organ systems where it is important for both intracellular and extracellular cell functions. ATP is a complex molecule which is composed of an adenosine molecule and three phosphate groups. Intracellular ATP is primarily utilized to drive energy required processes, for instance, active transport. As the 'energy currency' in the cell, ATP can release energy when one or two of the phosphate groups are removed [32]. Extracellular ATP is considered to act as a signaling molecule [33]. Signaling roles for ATP have been clearly established in several tissues, including the regulation of epithelial cell responses [34] [35] and the activation of platelets at sites of vascular injury [36]. Specifically, in bone cells, the release of

ATP can be trigger under various mechanical stimuli, such as shear stress, stretching, and hydrostatic pressure [37]. Thus, ATP appears to be a prone candidate for mediating intercellular communication in response to mechanical stimulation.

1.5 Goal

While mechanical stimulation of bone cells are widely studied using shear stress, stretching and local indentation techniques, the intercellular communication mechanism remains unknown. The goal of this thesis is to investigate the properties of ATP as an extracellular mediator released in response to mechanical stimulation of bone cells. This thesis is organized into four chapters, following the introduction. In Chapter 2, mathematical modeling is used to study the role of multiple P2 receptors, capable of binding to ATP and other nucleotides, as well as extracellular ATP degradation and diffusion. Chapter 3 provides the principle of direct detection of ATP using firefly luciferase chemiluminescence method, followed by the calibration with a luminometer. Chapter 4 focuses on direct ATP detection upon mechanical stimulation of osteoblasts with AFM. Finally, Chapter 5 summarizes the main results presented in this thesis.

CHAPTER 2
ATP Signaling Model

2.1 Overview of ATP signaling pathway

Extracellular ATP is known to act as a signaling mediator in many cell regulation processes [37]. Figure 2–1 illustrates a schematic graph of intercellular communication via soluble signaling mediators ATP, Adenosine Diphosphate (ADP) and Adenosine Monophosphate (AMP).

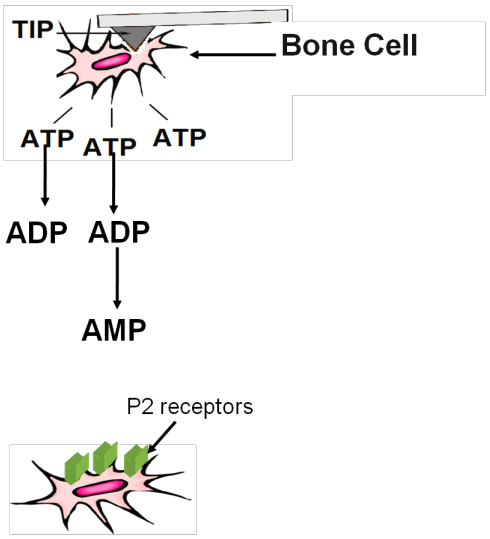

Figure 2–1: Schematics of intercellular signalling

The ATP signaling pathway consists of four steps:

- First, a bone cell is stimulated with a AFM cantilever tip. Transient ATP is then released from the punctured cell, here referred to as the primary cell, in the amount proportional to the extent of the injury.
- Secondly, ATP, a compound containing three phosphate molecules, diffuses and degrades into ADP and AMP by losing a phosphate molecule. The degradation reactions are facilitated by enzymes in the Nucleoside triphosphate diphosphohydrolase (NTPase) family on the cell surface.
- Thirdly, the signals are transmitted to another bone cell via P2 receptors on the cell membrane, shown in green. There are two families of P2 receptors: P2X, the ligand-gated ion channels, and P2Y, the G-protein-coupled receptors. P2X receptors are activated uniquely by ATP , whereas P2Y receptors can be activated by ATP, Adenosine Diphosphate (ADP), Uridine Triphosphate (UTP) and Uridine Diphosphate (UDP)[38]. In this thesis, only ATP signaling will be investigated.
- Finally, binding of ATP to P2 receptors triggers the intracellular signal cascade reaction, leading to changes inside the cells, including transient elevation of calcium.

2.1.1 ATP degradation and diffusion mechanism

Upon local indentation, ATP can be released from bone cells into the extracellular milieu. This represents an important component to initiate a signaling cascade [31]. Intracellularly, ATP is present at the highest concentrations, compared to other

nucleotides: 10 fold more ATP than ADP and 100 fold more ATP than AMP. Therefore, if nucleotides are released simply through the cell membrane, more ATP will be released compared to ADP and AMP. ATP can then diffuse through the extracellular fluid to the neighboring cells and activate the trans-membrane P2 receptors. Evidence of ATP presence in the extracellular milieu has been shown using agitation of cell suspensions [39] and direct addition of luciferase/luciferin reagent to the cells for sensing ATP in real time [34].

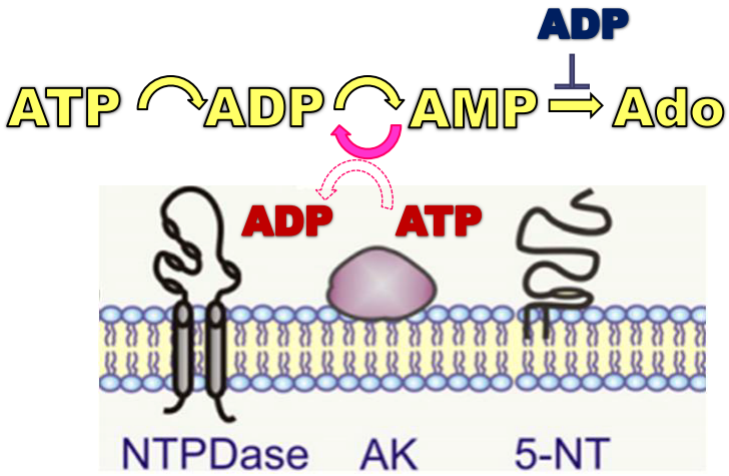

Figure 2–2: Schematic of ATP degradation cascade

Aside from diffusion, ATP is also hydrolyzed to ADP via enzymes in the NTPDase family [31]. A schematic of the degradation mechanism, which involves three major enzymes, is shown in Figure 2–2. The NTPDase enzyme family are capable of hydrolyzing both ATP and ADP by clipping off a phosphate molecule, but it is incapable of affecting AMP. Subsequently, AMP is hydrolyzed to adenosine via a member in the Ecto-5'-nucleotidase (5-NT) protein family, known as CD73 [40].

Furthermore, the degradation mechanism is regulated to avoid a sudden increase of adenosine in the cells, since an accumulation of adenosine is toxic to the cells [41]. Ecto -5'-nucleotidase is inhibited by the free ADP molecules in the extracellular environment, preventing AMP from binding to Ecto -5'-nucleotidase to generate excessive adenosine. In addition, a prominent intracellular regulator of ATP/ADP balance, adenylate kinase (AK), has been shown to be present extracellularly [31]. AK catalyzes the reversible reaction ATP + AMP $\longrightarrow$ 2ADP. Through these regulations, the adenosine level can be maintained at a steady level over various amount of ATP release.

2.1.2 P2 receptors

The third step of ATP signaling mechanism is signal receiving. In order to receive the information carried by ATP or other nucleotides, a set of transmemberane receptors, known as P2 receptors are activated through binding to ATP molecules and other nucleotides. Extracellular nucleotides are able to initiate cell signaling through two major receptor subfamilies: P2X and P2Y receptors. P2X ($P2X_1$ through $P2X_7$) receptors are ligand-gated ion channels [42]. When ATP binds to the P2X receptors, the ion channels change configuration and allow ions to flow into the cell. P2Y receptors, on the other hand, are a group of eight G-protein-coupled receptors, P2Y1, P2Y2, P2Y4, P2Y6, P2Y11, P2Y12, P2Y13, P2Y14. Unlike P2X receptors responding only to ATP, P2Y receptors can also be activated by ADP, UTP and UDP, however, in this thesis, only the signaling of ATP will be addressed. The ligand-receptor complex activates the G-protein which in turn actives the effectors protein.

The effectors protein is often an enzyme which can generate small second messenger molecules. The second messengers then activate a series of enzymes called kinases. The kinase phosphorylates and thus activates other enzymes which finally alter cell functions. The mechanism of P2Y receptors is shown in Figure 2–3.

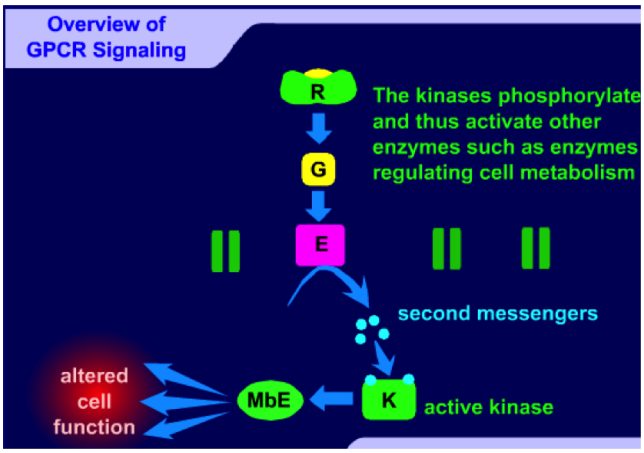

Figure 2–3: Schematic of G-protein coupled receptors signaling mechanism [3]

It is interesting to note that multiple P2X and P2Y receptors are expressed on osteoblasts ($P2X_{2,5,6,7}$ and $P2Y_{1,2,4}$) and osteoclasts ($P2X_{2,4,7}$ and $P2Y_{1,2,6}$) [42], however, it is not clear why so many receptors are needed and what are the specific roles for each of the receptors. In attempt to address these questions, a mathematical model is built to describe the behavior of receptors in response to different ATP concentrations.

2.2 Individual characteristics of P2 receptors

ATP dose response is an important characteristics of P2 receptors. Previously, individual receptor was over-expressed on the cell surface and its activity in response to different ATP concentrations was studied using whole cell patch clamp technique.[43] This technique involves applying a gentle suction with a pipette tip to lift a piece of cell membrane, forming a tight seal between the broken cell membrane and the tip wall. Different concentrations of ATP are then applied to the cells to activate P2 receptors. The ions passing through the receptors change the potential of the cell, which generate a current through the electrode inside the pipette tip. The amount of current generated is proportional to the percentage of activated P2 receptors. Hence, a ATP dose response curve for a single receptor can be generated, as shown in Figure 2–4(a).

Hill equation was applied to model ATP concentration dependence of P2 receptors. Hill equation describes the fraction of the macromolecule saturated by ligand as a function of the ligand concentration; it is used to determine the degree of cooperativity of the ligand binding to the enzyme or receptor [4]. The general formula for Hill equation is:

$$\theta = \frac{x^n}{K_{1/2}^n + x^n} \tag{2.1}$$

Where θ is the fraction of the receptors responded; x represents ligand concentration (M); $K_{1/2}$ is the ligand concentration at half maximum response and n represents the Hill coefficient, describing cooperativity.

In the case of P2 receptors, the ligand is ATP. The xy coordinates and the half maximum response value ($K_{1/2}$) of each receptor are estimated from experimental measurements found in literature [4]. The data is fitted to Hill equation with nonlinear least square fit in MatLab.

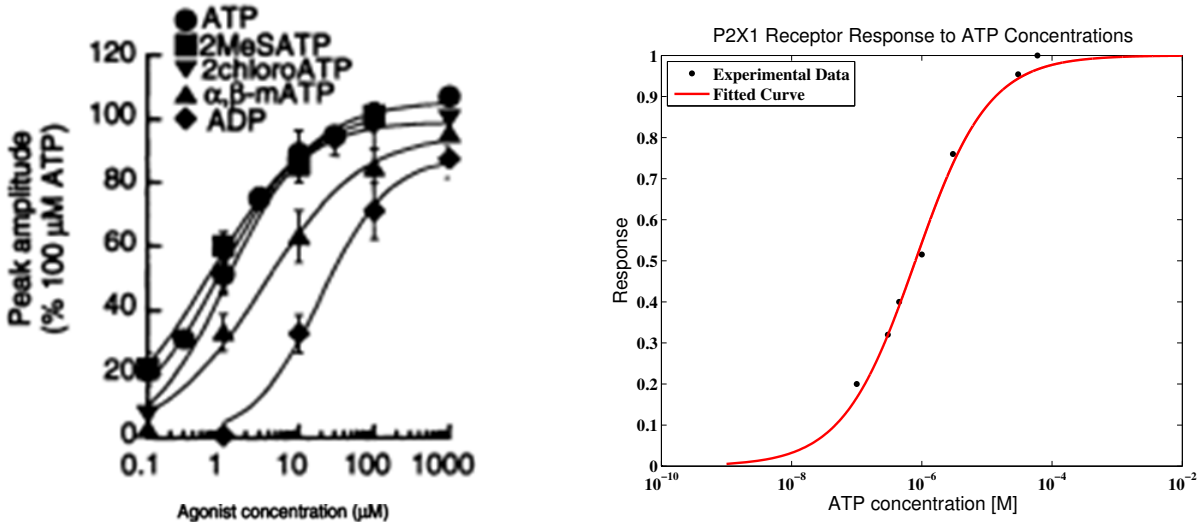

(a) (b)

Figure 2–4: (a)The experimental data taken from literature[4]. Peak amplitude versus different agonist concentrations are plotted, but only ATP data is used. The graph is normalized by dividing each peak amplitude value by the value corresponding to 100μM ATP. (b)Fitted curve to Hill equation. The black dots are experimental data points replotted in MatLab. The red line represents the non-linear fit curve in matlab which gives the Hill coefficient n=0.776.

Below the protocol for fitting of $P2X_1$ receptor is given as an example of the fitting process.

1. Superimpose an empty graph of the same xy scale with Figure 2–4(a). The xy coordinates of each data points are then extracted, demonstrated in Table 1.

[ATP] (μM)	0.1	0.3	0.4	1.0	3.0	30.1	59.7
Normalized Peak Amplitude	0.20	0.32	0.40	0.51	0.76	0.95	1.00

2. Using the nonlinear best fit function in Matlab to fit the data points to Hill equation, the following parameters are obtained:$K_{1/2}$=0.797μM, n=0.776 with R^2=0.9936. In statistics,R^2 provides a measure of how well outcomes are likely to be predicted by the current model [44]. R^2 =1 indicates that the fitted model explains all variability of the data; R^2=0 means there is no relationship.
3. The mathematical function of $P2X_1$ is determined to be $\theta_{P2X_1} = \frac{x^n}{K_{1/2}^n + L^n} = \frac{x^{0.776}}{(0.797\times10^{-6})^{0.776}+x^{0.776}}$, plotted in Fig.2–4(b).

The same method is applied to obtain the mathematical functions of all the other P2X and P2Y receptors. The fitted coefficients for each receptor are shown in Table 2–1. The function of P2 receptors in response to ATP are also plotted in Figure 2–5.

Table 2–1: Fitting parameters of P2 Receptors from Hill Equation $\theta = \frac{x^n}{K_{1/2}^n + x^n}$

P2 Receptors	Half maximum response $K_{1/2}$	Coefficient n	Reference
$P2X_1$	0.797×10^{-6}	0.776	[4]
$P2X_2$	11.0×10^{-6}	2.30	[45]
$P2X_3$	0.899×10^{-6}	1.42	[46]
$P2X_4$	7.17×10^{-6}	1.40	[43]
$P2X_5$	0.701×10^{-6}	0.70	[47]
$P2X_6$	A silent receptor, not activated by ATP		[48]
$P2X_7$	232×10^{-6}	1.66	[49]
$P2Y_1$	1.77×10^{-6}	0.96	[50]
$P2Y_2$	0.175×10^{-6}	1.00	[51]
$P2Y_4$	30.0×10^{-6}	1.12	[51]
$P2Y_6$	Activated by UDP instead of ATP		[31]
$P2Y_{11}$	3.85×10^{-6}	0.620	[52]
$P2Y_{12}$	4.10×10^{-6}	0.815	[53]
$P2Y_{13}$	Activated by ADP		[31]
$P2Y_{14}$	Activated by UDP instead of ATP		[54]

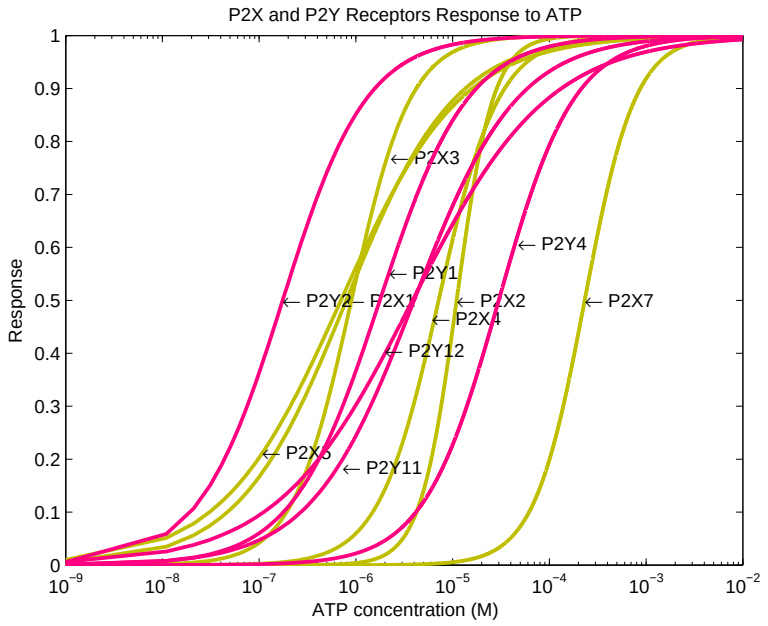

Figure 2–5: ATP dose dependence of P2X (yellow curves) and P2Y(red curves) receptors

In Figure 2–5, all the P2X receptors can be divided into 3 groups. $P2X_1$, $P2X_3$ and $P2X_5$ receptors are very similar; they react to small amount of ATP concentration below 1μM. $P2X_4$ and $P2X_2$ are activated by approximately 10 μM ATP. $P2X_7$ on the other hand are activated by much high concentration of ATP. Similar to P2X receptors, P2Y receptors can also be divided into 3 groups based on their response to ATP concentrations: 1) $P2Y_2$; 2) $P2Y_1$, $P2Y_{11}$, $P2Y_{12}$; and 3) $P2Y_4$. P2X and P2Y receptors cover ATP concentration range from 1 nM to 1 mM with approximately even steps. From 0.5 μM to 50 μM ATP, receptors activation is well resolved. With the exception of $P2Y_2$ and $P2X_7$, all the other receptors are active in this range. It is also interesting to note that P2X and P2Y receptors seem to alternate throughout, with P2Y receptors filling the concentration gaps of P2X receptors.

2.3 Roles of P2 Receptors on Osteoblasts

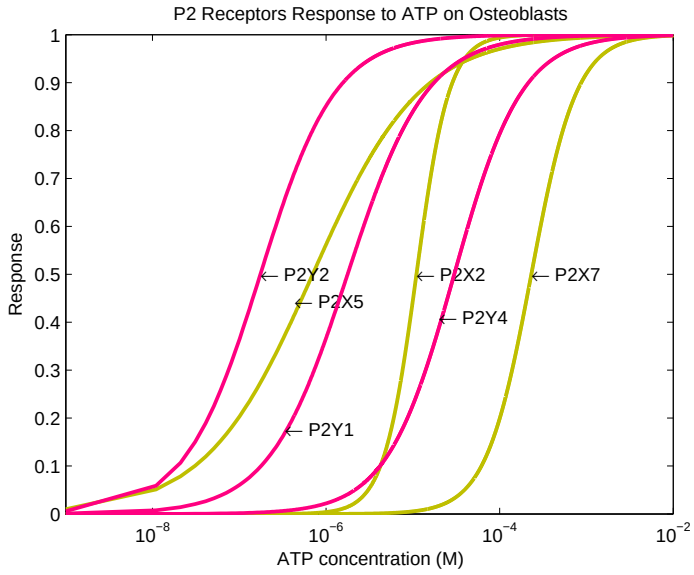

Figure 2–6: ATP concentration dependence for P2 receptors on osteoblasts. The red line and yellow lines represent P2Y receptors and P2X receptors respectively.

Next, we aim to access how individual receptors may contribute to ATP cellular response in a functional cell model, where multiple ATP receptors are present. On osteoblasts, only $P2Y_{1,2,4,6}$ and $P2X_{2,5,7}$ are expressed. These seven receptors are activated by a wide range concentration of ATP as shown in Figure 2–6. P2Y6 is not included, because it is a silent receptor with respect to ATP, activated by UDP. It is of interest to note that the two overall features of receptor distribution for all P2 receptors, shown in Figure 2–5, are maintained, even when only the receptors present on osteoblasts are plotted. First, large range of ATP concentration is covered; Second, P2X and P2Y receptors alternate within this range. Multiple receptors can

respond to the same range of ATP concentration. For example, 10^{-7}M to 10^{-6}M ATP can activate the first three receptors $P2Y_1$, $P2X_5$ and $P2Y_2$. A long standing question in the feed of P2 receptor signalling is that if multiple receptors can be activated by a similar ATP concentration, why a cell needs more than one receptor. In collaboration with Matthew Grol and Dr. Jeff Dixon from University of Western Ontario, we will investigate what the contribution of an individual receptors to the cellular response to different ATP concentration of a physiologically viable cell.

2.3.1 Experimental Data Demonstrates Complex, Non-Linear ATP Concentration Dependence

Through collaboration with Dr.Dixon and Matthew.Grol from University of Western Ontario, we received experimental data where they measured the increase of Ca^{2+} level in osteoblasts after the application of various ATP concentrations. The ATP concentrations used matches the exact ATP range(1nM to 10mM) in our P2 receptors model. In their experiment, a dish of cultured osteoblasts are pre-incubated with a calcium sensitive dye Fura-2 AM, which binds to free calcium inside the cell to produce light when excited to a certain wavelength. The dish of osteoblasts is then placed under a fluorescent optical microscope for real time imaging. First, a baseline calcium level is measured for 600s as control. A known concentration of ATP is then sprayed uniformly on the osteoblasts at the 600s mark. Finally,the calcium response is measured by the change in light intensity of individual cells. In Figure 2–7(a), 100μM ATP is sprayed onto a field of 15 osteoblasts. To ensure that ATP is evenly distributed among all the osteoblasts,the calcium responses for all 15 cells are plotted

with respect to imaging time. A sharp increase in calcium response is observed when ATP is added. Since the calcium level peaks at approximately 10mins for all 15 cells, one can conclude that the the ATP is uniformly distributed among the cells.

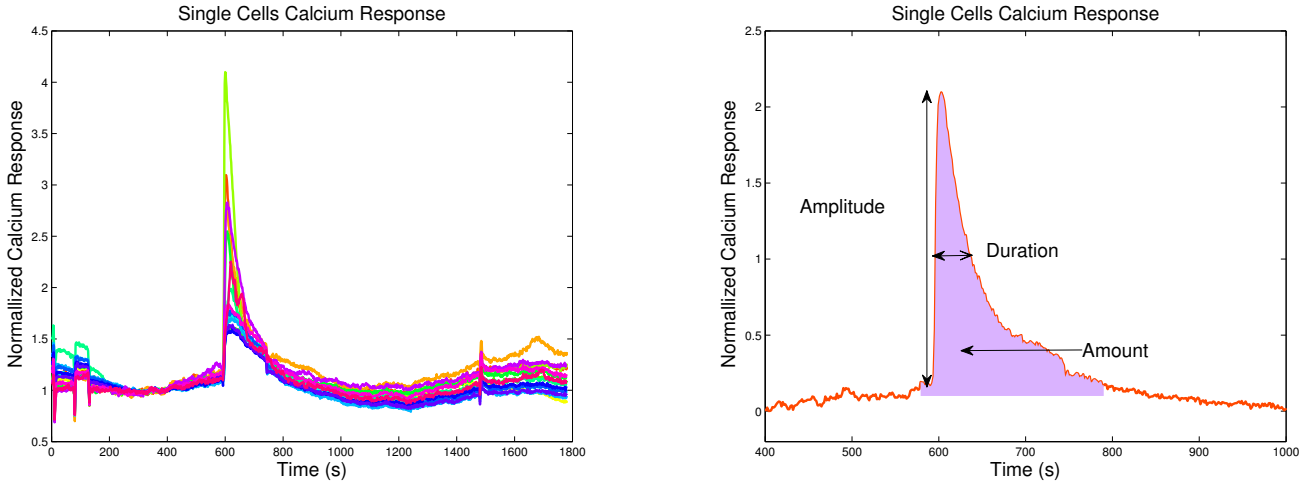

(a) (b)

Figure 2–7: Data Analysis of 100μM ATP stimulated single cell calcium response.(a)Single cells calcium response when 100μM ATP is sprayed on the imaging field of 15 osteoblasts.(b)The analysis of calcium response amplitude, duration and the calcium amount produced.

Three important pieces of information can be extracted from the raw data plot in Figure 2–7(a): the amplitude of calcium release, the duration of calcium response and the amount of calcium released by the cells over time. As indicated in Figure 2–7(b), the amplitude is calculated by subtracting the average of the background calcium level from the highest calcium response. The duration is determined by measuring the time difference between half maximum points on the rising and decaying parts

of the curve. Finally, the amount of calcium released by each cell is computed by integrating the area under the curve.

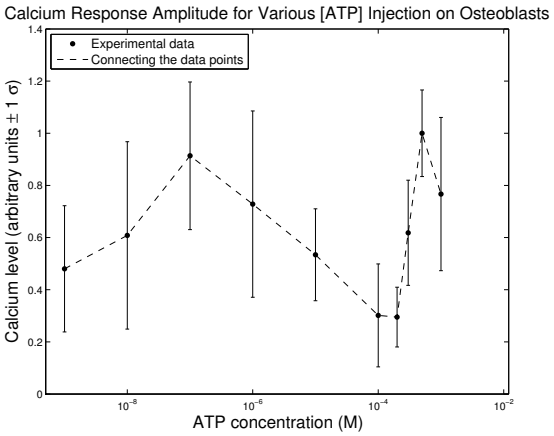

(a) Amplitude

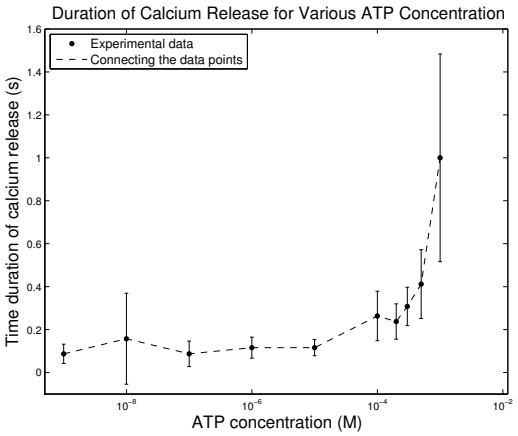

(b) Duration

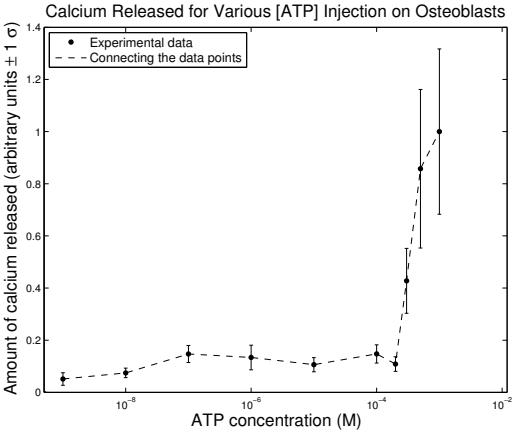

(c) Amount

Figure 2–8: Different concentrations of ATP are sprayed onto osteoblasts. The amplitude, duration and amount of calcium released are plotted with respect to ATP concentrations. Data points are means ± standard deviation, n=15 osteoblasts.

Averaging over 15 osteoblasts, amplitude, duration and amount of calcium released are plotted over a range of ATP concentrations, shown in Figure 2.3.1. All data sets are normalized by dividing the highest values over each data point. The standard deviation from the average is used as error bars on individual data point. The amplitude plot demonstrates an initial increase in calcium amplitude from 10^{-9} nM to 10^{-7} nM, followed by an amplitude decrease at 10^{-7} nM with increase of ATP concentration, finally an increase in amplitude again at 5×10^{-7} nM . The duration curve only has a final rise when ATP concentration reaches 10^{-4}M . Figure 2–8(c) indicates two increases for the amount of calcium released, over a range of ATP concentrations. The first increase occurs when approximately 10^{-7} M ATP is sprayed onto the cells. The second increase appears when approximately 10^{-4} M ATP is added, at the same concentration as the duration curve starts to peak.

2.3.2 Modeling Hypothesis and Method

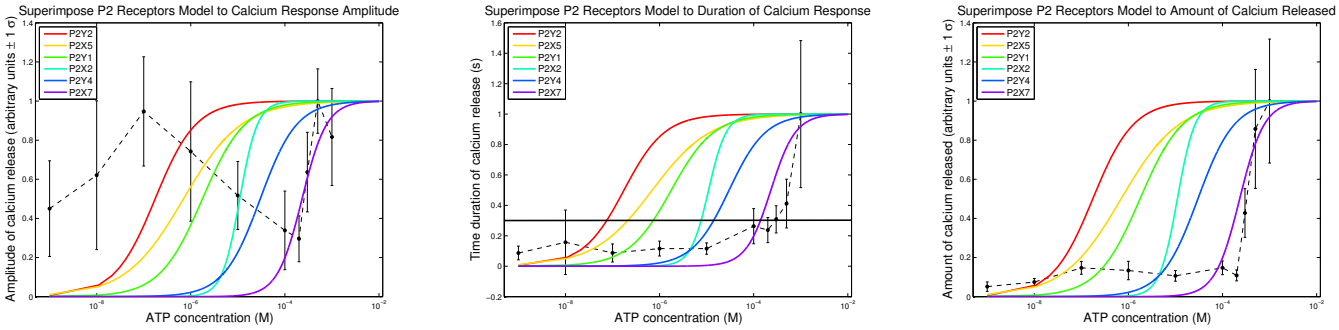

(a) Amplitude (b) Duration (c) Amount

Figure 2–9: This graph shows the superimpose of the P2 receptors model onto the analyzed experimental data for amplitude, duration and amount of calcium released.

In order to investigate the contribution of each receptor, the amplitude, duration and amount of calcium released are assumed to be proportional to the number of receptors activated. Hence, we are able to superimpose the analyzed experimental data with the P2 receptors modeling curves, as illustrated in Figure 2–9. These combinations demonstrate that Ca^{2+} response are obtained with the same ATP concentration range as individual concentration dependence for P2 receptors. Therefore, we hypothesize that the linear combination of these P2 receptor functions will fit the amplitude, duration and calcium amount curve. The ATP dose dependence for each P2 receptors present on osteoblasts have already been expressed using Hill equation in Section 2.2. The general equation for the linear combination fit is the following:

$$\theta_{total}(x) = k_1 \cdot P2Y_2 + k_2 \cdot P2X_5 + k_3 \cdot P2Y_1 + k_4 \cdot P2X_2 + k_5 \cdot P2Y_4 + k_6 \cdot P2X_7 \quad (2.2)$$

where k_1,k_2,k_3,k_4,k_5,k_6 are the coefficients for the linear combination. These coefficients represent the amount of contribution each receptor has towards the calcium response, at a certain ATP concentration.

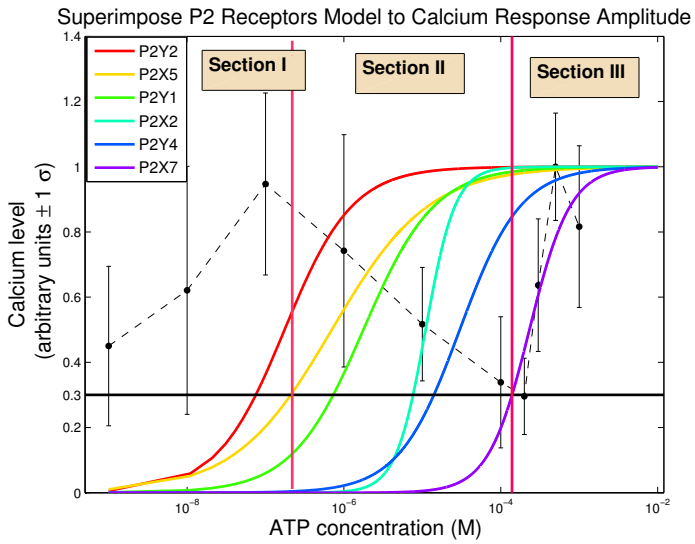

Figure 2–10: Schematic of dividing analyzed Ca^{2+} amplitude curve into three sections for characterization. The black dots represent the experimental data for ATP response, color curves represent individual receptors does dependence. The black line at y=0.3 indicates receptor activation threshold.

The next step is to fit the analyzed amplitude, duration and calcium amount curves with $\theta_{total}(x)$. In order to make an educated guess for the initial values of each fitting parameters, each curve is divided into three sections and fitted section by section. For instance, Figure 2–10 demonstrated the section division for the amplitude of calcium response curve, according to the rising and decaying trend of the experimental curve. Section I represents the first increase of the amplitude in the experimental data, Section II represents the decay and Section III represent the second increase in amplitude. We consider a receptor to be active when ATP has triggered at an arbitrary value of 30% of its response. In Section I, which contains

the first three data points, only $P2Y_2$ receptor is activated. In Section II,$P2X_5$, and $P2Y_1$, $P2X_2$, and $P2Y_4$ receptors are activated. Finally, in Section III, $P2X_7$ receptor is activated. .

2.3.3 Results

Fitting of Amplitude Curve

Section I contains 4 data points and only $P2Y_2$ receptor is activated. An inconsistency occurs here, where the actual data rises earlier than the modeled $P2Y_2$ receptor curve shown in red in Figure 2–10. In order to fit the actual data, the $P2Y_2$ receptor curve must be shifted to the left. This limitation could be due to the fact that the data we used to model P2 receptors are obtained from transfected cells, causing a certain type of receptors to be overly expressed, for measurement purpose. The experimental data from Dr. Dixon's group, however, are done with primary, non-transfected cells. Therefore, the $P2Y_2$ concentration dependence is shifted to the left, by decreasing the values of $K_{1/2}$ and n.

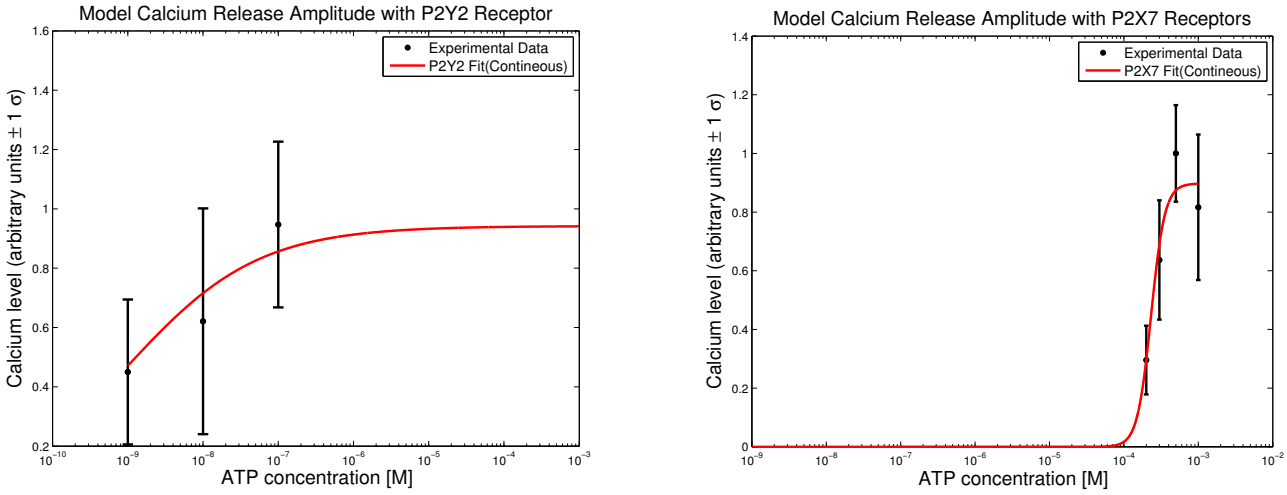

(a) (b)

Figure 2–11: (a) Section one is fitted with $P2Y_2$ receptors function only. k_1=0.94, R^2=0.86 (b) Section three is fitted with $P2X_7$ receptor function. k_6=0.90, R^2=0.91. The black dots represents experimental data and the red line is the fitted curve.

The first 4 points of section one are fitted with the corrected $P2Y_2$ receptor function (Eq.2.3), as demonstrated in Figure 2–11(a).

$$k_1 \times P2Y_2 = k_1 \times \frac{x^{0.5}}{(0.001 \times 10^{-6})^{0.5} + x^{0.5}} \tag{2.3}$$

All the fitted coefficients are within 95% confidence. The positive k_1=0.94 coefficient implies that $P2Y_2$ is responsible for the increase in the data points; and the R^2=0.86 indicates the function of $P2Y_2$ receptor can accurately describe the data sets. Next, we consider the last 4 data points in section three. $P2X_7$ appears to be

the only receptor whose activation threshold is within this range. Similar to $P2Y_2$ receptor, $P2X_7$ receptor function is also adjusted by increasing its cooperativity shown in Eq.2.4

$$k_6 \times P2X_7 = k_6 \times \frac{x^{4.7}}{(232 \times 10^{-6})^{4.7} + x^{4.7}} \tag{2.4}$$

The R^2=0.91 of the fitted curve in Figure 2–11(b) suggests that $P2X_7$ alone is capable of describing the overshoot in section three. Considering that section one and section three contain the majority of the data set on the amplitude of calcium release, we speculate that the linear combination of both receptors is able to describe the entire data set. Yet, the fitting with both $P2Y_2$ and $P2X_7$ receptors in Figure 2–12 has not presented an adequate fit, with a R^2 approximately 0. This suggests that other receptors are necessary to accurately construct the entire data sets.

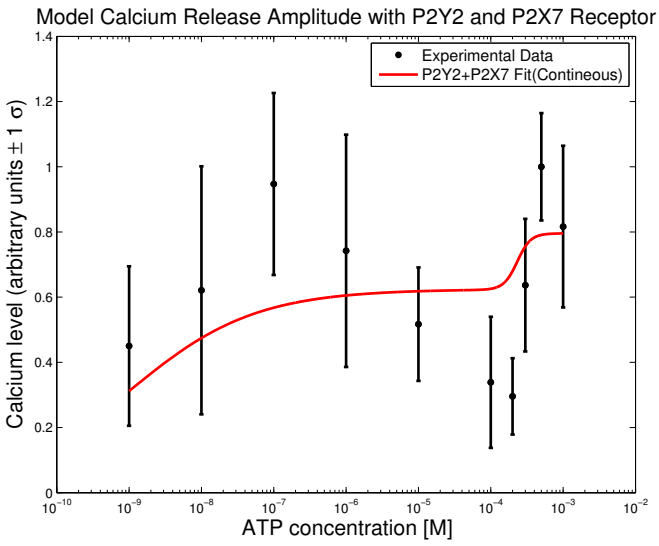

Figure 2–12: The data set on amplitude of calcium release is fitted with $P2Y_2$ and $P2X_7$ receptors. The R^2 of this fit is 0.046.

$P2X_5$, $P2Y_1$, $P2X_2$ and $P2Y_4$ are the receptors potentially activated by the intermediate concentration range of ATP in section two. In the interest of determining the role of each receptor, these 4 receptors are fitted separately to the amplitude date set.

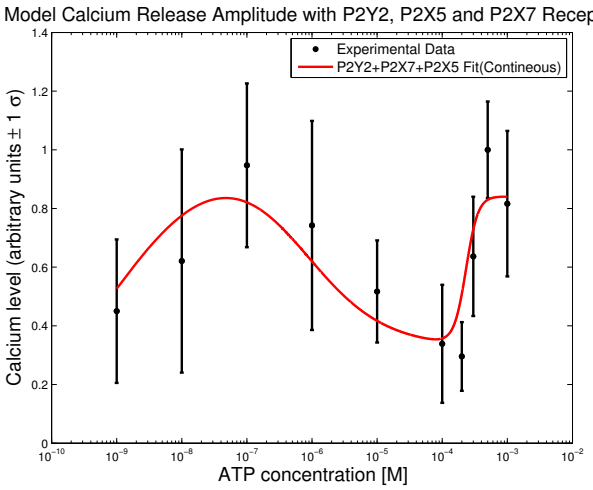

(a)

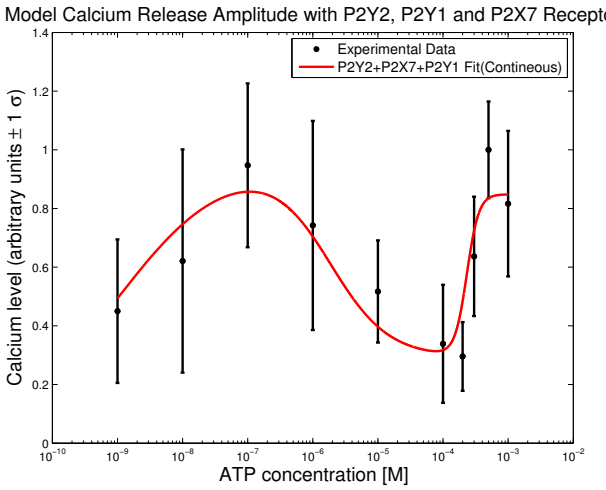

(b)

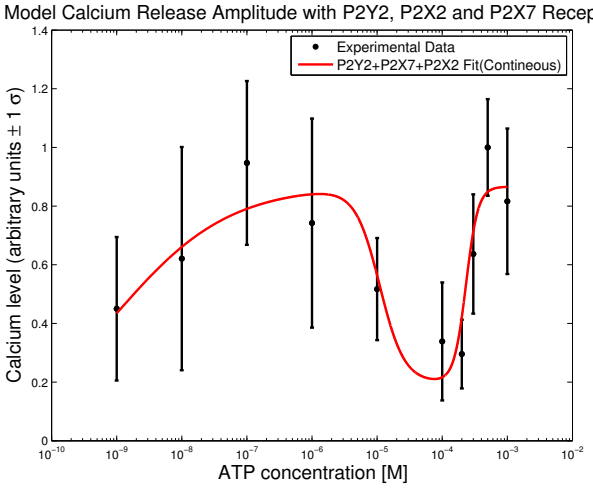

(c)

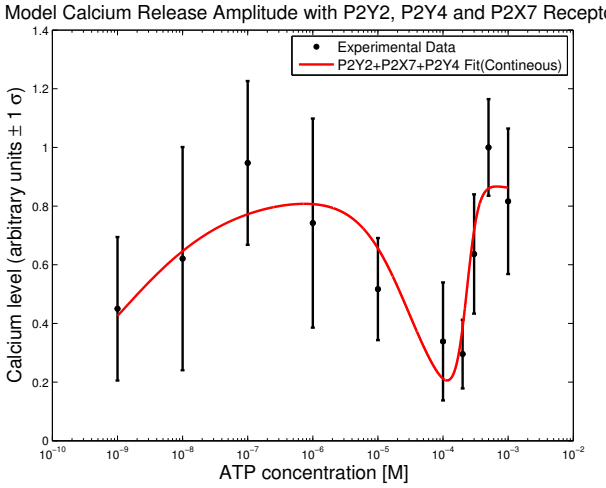

(d)

Figure 2–13: The amplitude data is fitted with $P2Y_2$, $P2X_7$ and the four receptors in section two individually.(a) The amplitude data set is fitted with $P2Y_2$, $P2X_7$ and $P2X_5$ receptors. The R^2 of the fit is 0.71. The coefficient of k_5 =-0.74 (b) $P2Y_2$, $P2X_7$ and $P2Y_1$ receptors fit: R^2 = 0.78, k_3 =-0.70 (c) $P2Y_2$, $P2X_7$ and $P2X_2$ receptors fit:R^2 =0.81, k_4 =-0.67 (d) $P2Y_2$, $P2X_7$ and $P2Y_4$ receptors fit: R^2 =0.79, k_5 =-0.82

Among the four fitted curves in Figure 2–13, the fit with $P2X_5$ (Fig.2–13(a)) and $P2Y_1$ (Fig.2–13(b)) are similar in shape. $P2X_2$ (Fig.2–13(c)) and $P2Y_4$ (Fig.2–13(d)), on the other hand, create a bigger dip at the local minimum. Despite of these differences, all four receptors can justify the decaying part of the data set. Importantly, the linear coefficients for each of them appears negative, which indicates that they have an inhibitory effect on the amplitude of calcium response.

Fitting of Duration Curve

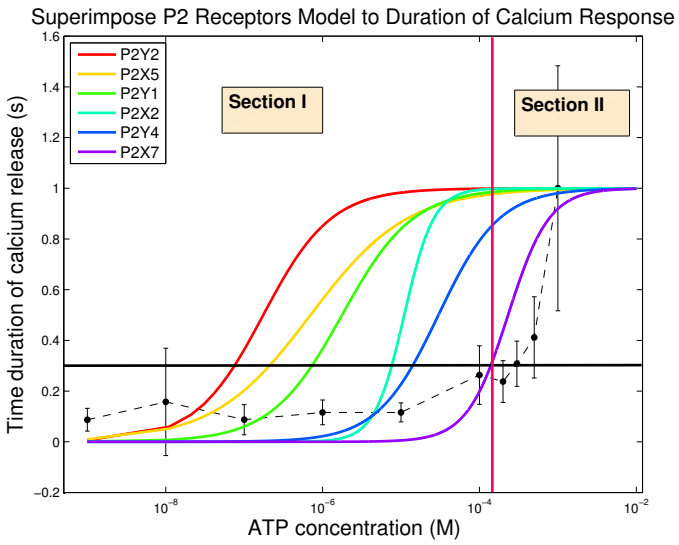

Figure 2–14: Schematic of dividing analyzed Ca^{2+} duration curve into two sections for characterization. The black dots represent the experimental data for ATP response, color curves represent individual receptors does dependence. The black line at y=0.3 indicates that a receptor is considered active, when sufficient ATP can trigger 30% of the receptors.

Unlike the amplitude curve, the duration of calcium response data only has an increase, when the ATP concentration reaches approximately 10^{-4} M. Following the same general strategy as the described in the previous section, the duration data are divided into two sections, illustrated in Figure 2–14. Also, it is of interest to note that only $P2X_7$ are activated in section two and all the other receptors are triggered in section one.

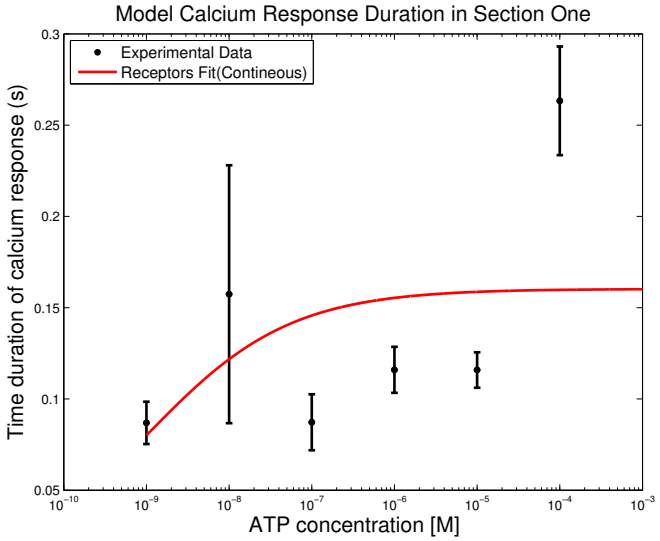

Figure 2–15: Section one of the duration data of calcium response is fitted with $P2Y_2$, $P2X_5$, $P2Y_1$, $P2X_2$ and $P2Y_4$ receptors. The R^2 of this fit is 0.15.

In section one, the duration data is fitted with $P2Y_2$, $P2X_5$, $P2Y_1$, $P2X_2$ and $P2Y_4$ receptors, shown in Figure 2–15. The low R^2 of 0.15 indicates that at low concentration of ATP, the duration of the calcium response is independent of the number of activated receptors. Furthermore, this part of the data is close to a flat

line, except for a small increase at the last data point. This suggests that the duration of calcium response is also independent of ATP concentration.

Considering $P2X_7$ is the sole receptor that is activated in section two of the duration data and calcium response duration is independent of all the other receptors, we decide to fit the entire duration data set with $P2X_7$ receptors curve. A constant β is added to the $P2X_7$ receptor function, because the base line of the duration curve starts at approximately 0.1, whereas the receptor curves start at 0. The following equation (Eq.2.5) is used to fit the duration data set.

$$k_6 \times P2X_7 + \beta = k_6 \times \frac{x^{4.7}}{(232 \times 10^{-6})^{4.7} + x^{4.7}} + \beta \tag{2.5}$$

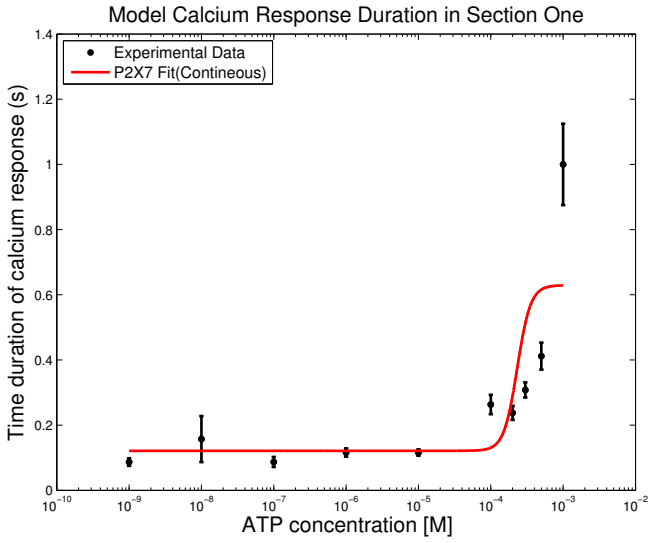

Figure 2–16: The duration data of calcium response is fitted with $P2X_7$ receptor. The R^2 of this fit is 0.64. $\beta = 0.1$.

Figure 2–16 reveals that only $P2X_7$ appears to affect the duration of the calcium response. At low ATP concentration, while $P2X_7$ receptors are not activated, the duration is independent of ATP concentration. Yet, at high ATP concentration (10^{-4} M), the duration of the calcium response increases proportionally to the number of activated $P2X_7$ receptors.

Fitting of Calcium Amount

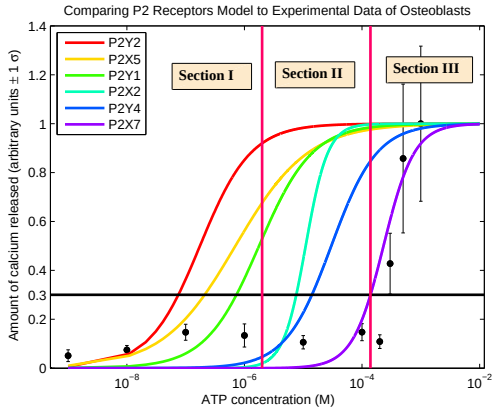

Figure 2–17: Schematic of dividing analyzed Ca^{2+} amount curve into three sections for characterization. The black dots represent the experimental data for ATP response, color curves represent individual receptors does dependence. The black line at y=0.3 indicates that a receptor is considered active, when sufficient ATP can trigger 30% of the receptors.

The calcium amount data is divided into three sections, based on the rising and decaying trend of the experimental curve. Section I represents the first increase of

Ca^{2+} levels in the experimental data, Section II represents the plateau and Section III represent the second increase Ca^{2+} .

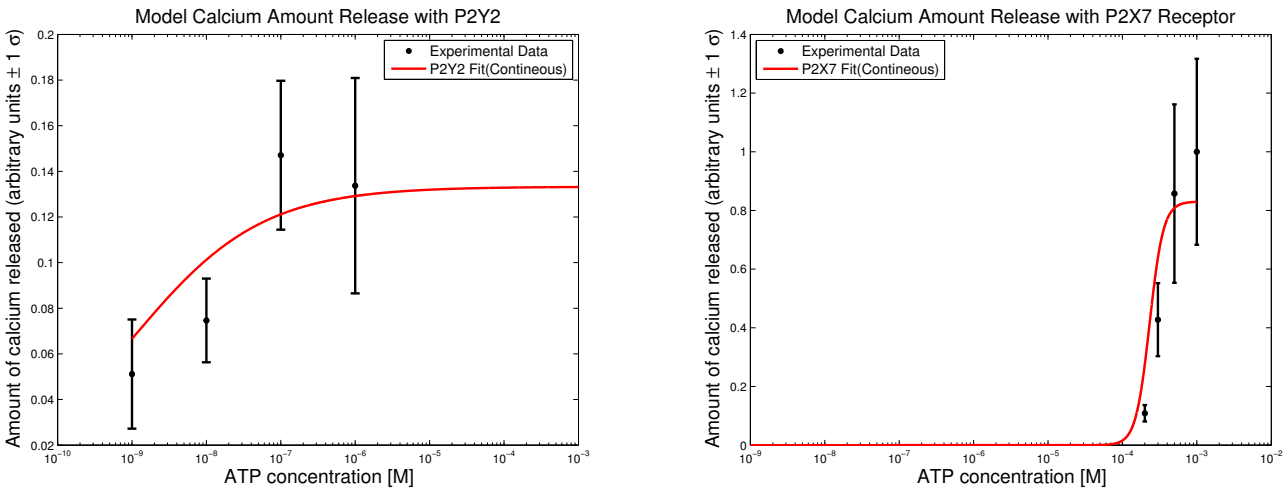

(a) (b)

Figure 2–18: (a)Section one is fitted with $P2Y_2$ receptor. The R^2 of this fit is 0.74.(b)Section three is fitted with $P2X_7$ receptor. The R^2 of this fit is 0.79.

First, the four data points from section one is fitted with $P2Y_2$ receptors. Looking at Figure 2–20(a), one can conclude that $P2Y_2$ receptor function is able to describe this part of the data. This means that $P2Y_2$ receptor is responsible for the first increase in calcium amount in the experimental data. In section one, $P2X_5$ and $P2Y_1$ receptors also appears to activated, however, their contribution adds very little to the fitting with $P2Y_2$ alone. Therefore, the fit of the other two receptors are not plotted here. Next, $P2X_7$ receptor is fitted to the last four data points from section three. The R^2= 0.79 of this fit also suggest that $P2X_7$ is responsible for the second great increase in the calcium amount data.

Since $P2Y_2$ and $P2X_7$ receptors are capable of describing section one and section three of the calcium amount data, one would suspect that if the linear combination of these two receptors can describe the entire data sets. Figure 2–19 proves this speculation. Adding all the other receptors does not improve this fit (fitting not shown here).

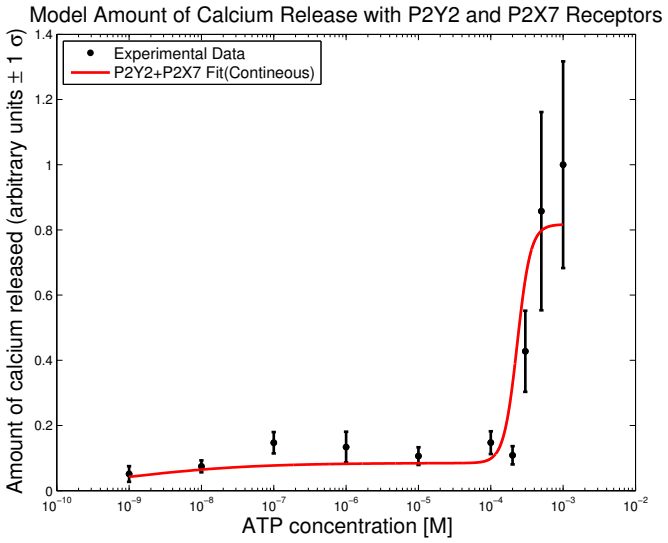

Figure 2–19: The amount of calcium release data is fitted with $P2Y_2$ and $P2X_7$ only. The R^2 is equal to 0.87

2.3.4 Partial conclusion

To summarize, fitting the P2 receptors data to actual experimental data allows us to determine the role of each receptor. From the fittings to amplitude, duration and amount data, one can conclude that:

- $P2Y_2$ receptor is responsible for the initial calcium increase in the amount curve

- $P2X_7$ receptor affects both calcium amount and calcium response duration.
- All the other receptors have an inhibitory effect on the calcium response.

2.4 Modeling of ATP Degradation and Diffusion

When ATP is released from the mechanically stimulated cell, it has to diffuse through the extracellular matrix to reach the P2 receptors on the neighboring cells. In addition, multiple enzymes present on the cells surface degrade ATP to ADP, AMP and adenosin, as described previously in section 2.1.1. The goal of the next study is to build a mathematical model describing ATP release, diffusion and degradation.

2.4.1 Diffusion equation

ATP, ADP and AMP diffuse between osteoclasts. Its behavior can be described by the Diffusion equation:

$$\frac{\partial c}{\partial t} = D\frac{\partial^2 c}{\partial x^2} \tag{2.6}$$

where c represents the concentration of the substance and D represents the diffusion coefficient, which is defined by the amount of a particular substance that diffuses across an unit area in 1 second.[55]

Therefore, ATP, ADP and AMP diffusion can be described as

$$\frac{\partial c_i}{\partial t} = D_i\frac{\partial^2 c_i}{\partial x_i^2} \qquad (i = 1, 2, 3) \tag{2.7}$$

where c_i represents the concentration of the mediators ATP, ADP and AMP. D_i represents the diffusion coefficients of ATP, ADP and AMP. In this study, the diffusion coefficients of ATP, ADP and AMP are taken from literature to be $180\mu m^2/s$, $207\mu m^2/s$,$300\mu m^2/s$ respectively.[56]

2.4.2 Reaction kinetics

While ATP, ADP and AMP diffuse through the extracellular space, ATP can also degrade into ADP and AMP.

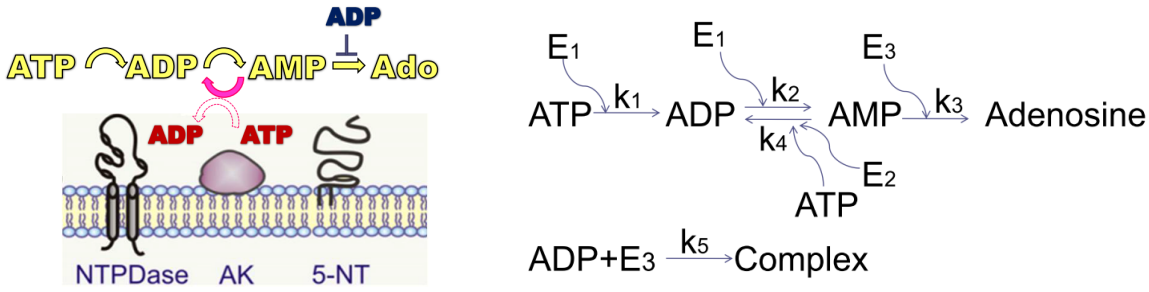

(a) (b)

Figure 2–20: (a)Schematic of ATP degradation with different enzymes.(b) ATP degradation reaction mechanism according to the schematic on the left. The k parameters represent the reaction rate.

Fig.2–20 shows the detailed mechanism of ATP, ADP and AMP degradation with the help of specific enzymes. Nucleoside triphosphate diphosphohydrolase (NTPDase) labeled as E_1 cleaves off an phosphate molecule to dephosphorylate ATP to ADP and ADP to AMP. We notice that the reaction from ADP to AMP is reversible. With the help Adenylate kinase (E_2), one molecule of ATP can bind

to another molecule of AMP reproduce two molecules of ADP. Finally, AMP degrades to Adenosine via Ecto-5'-nucleotidase (E_3). It is interesting to note that the activities of Ecto-5'-nucleotidase is regulated by free ADP. ADP can bind to Ecto-5'-nucleotidase to prevent the degradation of AMP to adenosine to avoid the accumulation of adenosine in the extracellular space. However, at the first step of model development, the inhibition mechanism is not taken into consideration in this study.

Therefore, the ATP, ADP and AMP degradation can be described by a set of differential equations.[55]

$$\frac{\partial c_1}{\partial t} = -c_1 e_1 k_1 - c_1 c_3 e_2 k_4 \tag{2.8}$$

$$\frac{\partial c_2}{\partial t} = c_1 e_1 k_1 - c_2 e_1 k_2 + 2c_1 c_3 e_2 k_4 - c_2 e_3 k_5 \tag{2.9}$$

$$\frac{\partial c_3}{\partial t} = -c_2 e_1 k_2 - c_1 c_3 e_2 k_4 - c_3 e_3 k_3 \tag{2.10}$$

where c_1, c_2 and c_3 are the concentration of ATP, ADP and AMP respectively. k_1, k_2, k_3,k_4 and k_5 represent the rate constants of each step of reaction as shown in Fig.2–20. Their values are taken from experimental data on smooth muscle cells in literature.[5] e_1,e_2 and e_3 are the concentration of enzymes of E_1,E_2 and E_3 respectively, but since we are only concerned with ATP diffusion and degradation, we will

not focus on the detailed effect of enzymes. All the enzyme concentrations are set to be 1 in this model.

2.4.3 Model

Combining both diffusion and degradation of ATP described in section 2.1 and 2.2, the final model of ATP signaling is described by a group of Partial differential equations (PDE).

$$\frac{\partial c_1}{\partial t} = D_1 \frac{\partial^2 c_1}{\partial x_1^2} - c_1 e_1 k_1 - c_1 c_3 e_2 k_4 \tag{2.11}$$

$$\frac{\partial c_2}{\partial t} = D_2 \frac{\partial^2 c_2}{\partial x_2^2} + c_1 e_1 k_1 - c_2 e_1 k_2 + 2 c_1 c_3 e_2 k_4 - c_2 e_3 k_5 \tag{2.12}$$

$$\frac{\partial c_3}{\partial t} = D_3 \frac{\partial^2 c_3}{\partial x_3^2} - c_2 e_1 k_2 - c_1 c_3 e_2 k_4 - c_3 e_3 k_3 \tag{2.13}$$

To solve the PDEs, initial conditions and boundary conditions have to be established. According to experimental data[5], we set the initial conditions of ATP, ADP and AMP, assuming at the source cell, only ATP is release:

$$c_{1i} = 500 \mu M \tag{2.14}$$

$$c_{2i} = 0 \mu M \tag{2.15}$$

$$c_{3i} = 0 \mu M \tag{2.16}$$

Boundary conditions:

$$\frac{\partial c_i(0)}{\partial x} = 1 \tag{2.17}$$

$$\frac{\partial c_i(500)}{\partial x} = 0 \tag{2.18}$$

Numerical analysis of this system is performed by programing this group of PDE with initial and boundary conditions using Matlab. Detailed Matlab code is shown in the Appendix.

2.4.4 Result and Discussion

ATP Diffusion only

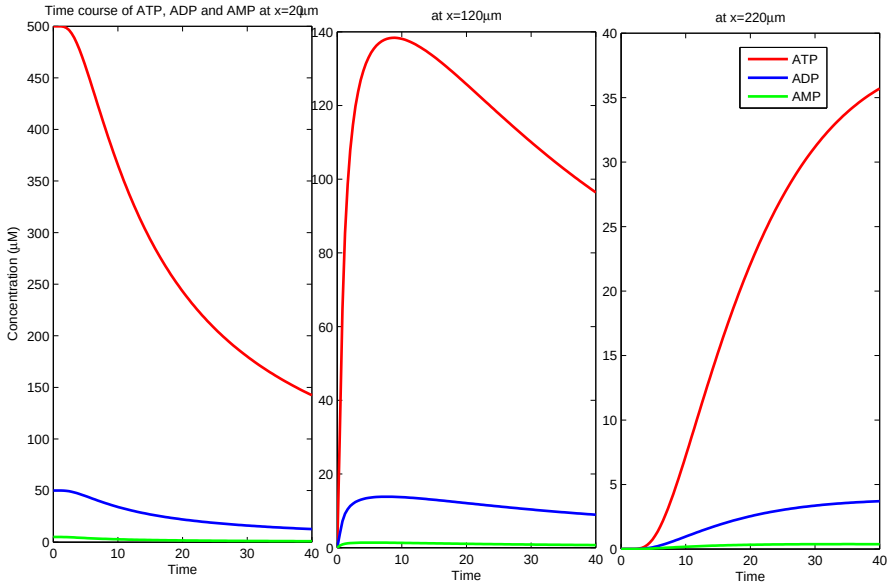

Figure 2–21: ATP, ADP and AMP diffusion ONLY curves over $20\mu m$,$120\mu m$ and $220\mu m$ away from the cantilever contact point. The red curves represent the concentration change of ATP; the blue curves represent ADP and the green curves represent AMP.

We set the contact point of AFM cantilever with the deformed cell to be the origin. In Figure.2–21, the three graphs represent the ATP, ADP and AMP diffusion behavior at distance 20 μm, 120 μm and 220 μm away from the contact point. We first simulated the model assuming that only diffusion is happening in the extracellular space, and all the reaction rate constants are set to 0 (k_i=0). The initial concentration of ATP , ADP and AMP are adjusted to be $500\mu M$, $50\mu M$ and $5\mu M$

respectively, because the initial condition of ADP and AMP can not be 0. As the mediators move further away from the source cell, the concentrations of ATP, ADP and AMP decrease with time and distance.

ATP diffusion and degradation

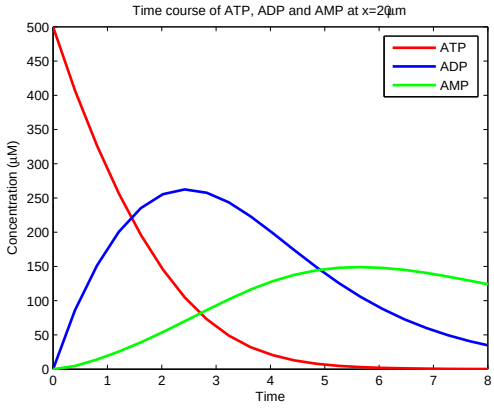

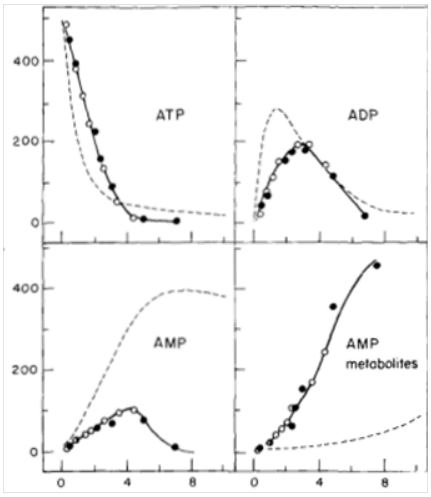

(a) (b)

Figure 2–22: (a)This graph shows the simulation of ATP, ADP and AMP diffusion and degradation model. (b) The experimental data of ATP, ADP, AMP concentration [5].

Next, we include ATP degradation process into the model. The left graph in Fig.2–22 shows the simulation of ATP, ADP and AMP diffusion and degradation model at 20 μm from the contact point. The initial concentrations of ATP, ADP and AMP are set to be 500 μM, 0 μM and 0 μM, since at the set of the injury, there is no ADP or AMP released. ATP, ADP and AMP exhibit time dependent

change in concentration. At approximately 2.5 seconds, ADP concentration exceeds ATP and AMP concentrations and at approximately 7 seconds, the concentration of AMP becomes the greatest of all three.

We compared these data to experimental findings. The graph on the right is plotted by experimental data taken from literature.[5] The hard lines in the graph represent the ATP, ADP and AMP concentration change with respect to time. Since ATP degradation act differently with different cell types, it is very difficult to compare the simulation results with experimental data quantitatively, however, The general time dependence of ATP and ADP from the simulation nicely fits the experimental data. The AMP curve from the experimental data is slightly shifted to the left comparing with our model simulation. This can be accounted for the fact that we did not take the inhibition of Ecto-5'-nucleotidase into consideration in the model. In reality, excessive ADP may bind to Ecto-5'-nucleotidase to prevent the conversion from AMP to adenosine which would cause the accumulation in AMP molecules. These may explain why the experimental data seems to have a peak of AMP earlier than the simulation.

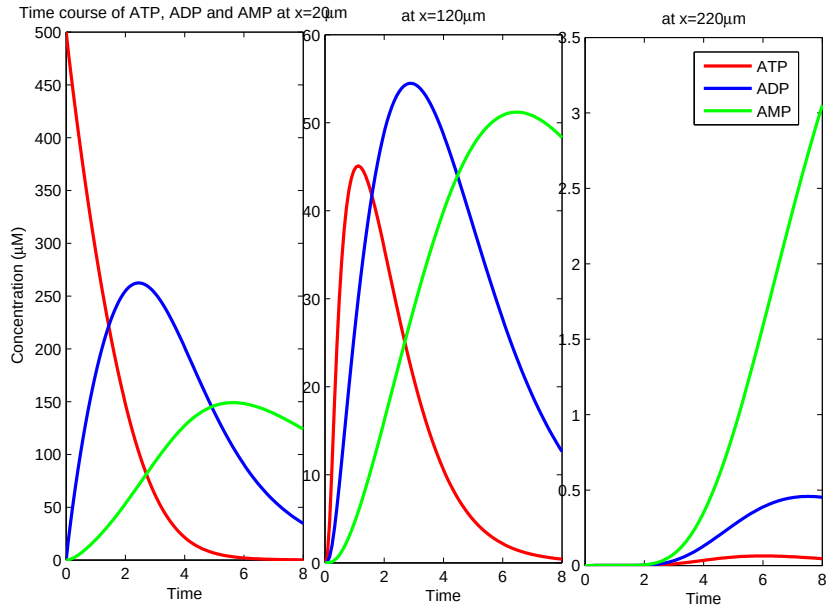

Figure 2–23: ATP, ADP and AMP diffusion and degradation over 20 μm,120 μm and 220 μm

Finally, we examine how taking into account diffusion and degradation of ATP affects the profile of ATP, ADP and AMP at different distance from the source of ATP release. Figure.2–22 proves that our model is an adequate representation of experimental data. In Figure.2–23, ATP, ADP and AMP diffusion and degradation over different distances are simulated. The initial concentrations of ATP, ADP and AMP are set to be 500 μM, 0 μM and 0 μM. At distance 20 μm from the contact point, the concentration of ATP is the highest. Thus, at 20 μm from the source, ATP represents the main mediator. However, at distance 120 μm from the contact point, the concentration of ATP decreases significantly. ADP concentration exceeds ATP concentration which allows ADP to become the main mediator of intercellular

signaling. Finally at 220 μm, the concentration of AMP is higher then both ATP and ADP concentration. We can conclude from this simulation that at different distances from the contact point, the main signal mediator changes from ATP to ADP to AMP.

In conclusion, the model developed is able to describe ATP diffusion and degradation mechanism. After mechanical stimulation, ATP is released from the source cell. The concentration of ATP, ADP and AMP decrease with time and distance at diffusion. Due to ATP degradation, the main propagating mediator may change from ATP to ADP to AMP over different distance. To improve the model, the inhibition of enzyme Ecto-5'-nucleotidase should be included in the model to improve the AMP concentration curve. Also, the concentrations of each enzymes involved in the degradation reactions should be accounted for to increase to accuracy of this model.

CHAPTER 3
Experimental Studies of ATP Measurements

The success in modeling of extracellular ATP signaling has stimulated a large interest in directly measuring ATP during the mechanical stimulation of osteoblasts. The direct measurement will serve as a concrete proof of that upon injury, ATP acts as the extracellular signal mediator. Chemiluminescence (CL) is widely employed for direct detection of ATP [31] [57] [58]. The term 'chemiluminescence' refers to light emission caused by a chemical reaction. Depending on the amount of light emitted from the chemical reaction, the corresponding ATP concentration can be determined. Thus, before performing imaging ATP during mechanical stimulation of osteoblasts, the first step is to test the CL approach via calibration of light emission over a series of ATP concentrations. The calibration is done using an instrument called a luminometer. In this chapter, we will first discuss the principles behind ATP imaging, followed by a description of cell preparation, and finally the calibration of ATP with the luminometer.

3.1 ATP Imaging with Luciferase

Firefly luciferase is an enzyme which catalyzes the chemical reaction of the firefly luciferase CL assay. Using this assay, a detection limit of 10^{-11} M ATP can

be achieved [59]. The following chemical reaction (Eq.3.1) is the governing reaction for detecting ATP with firefly luciferase CL.

$$D{-}luciferin{+}ATP{+}O_2 \xrightarrow[Mg^{2+}]{luciferase} oxyluciferin{+}AMP{+}pyrophosphate{+}CO_2{+}light \tag{3.1}$$

In the presence of the enzyme firefly luciferase, substrate D-luciferin reacts with ATP and Mg^{2+} to form oxyluciferin in its excited state. The excited oxyluciferin then decays to the ground state accompanied by an emission of photons. The maximum photon emission is approximately 560 nm [58]. When there is sufficient amount of substrate D-luciferin, ATP becomes the limiting factor of the reaction. Thus, the amount of light emitted is directly proportional to the amount of ATP. In other words, one can easily quantify the amount of ATP by measuring the intensity of light with this reaction.

3.2 Cell culturing and preparation

The mouse osteoblastic cell line C2C12 cells (American Type Ceulture) are cultured in DMEM (Dulbecoo's Modified Eagle Medium), supplemented with 10% fetal bovine serum (Wisent Inc. Cat. No.080140), 1% penicillin-streptomycin (Wisent Inc. Cat. No. 440-201-EL) and 1% sodium pyruvate (Wisent Inc. Cat.No.600-11-EL). This medium creates an optimum living environment and sufficient nutrients for the cells. Three days before the experiment, osteoblasts are plated onto 35 mm glass bottom dishes at 3×10^4 cells/cm^2. These dishes are then incubated in a condition

of 37^oC and 5% carbon dioxide (CO_2). These cells are supplied with fresh media every 48 hours until the experiment.

3.3 Preparation of ATP calibration curve

3.3.1 Luminometer

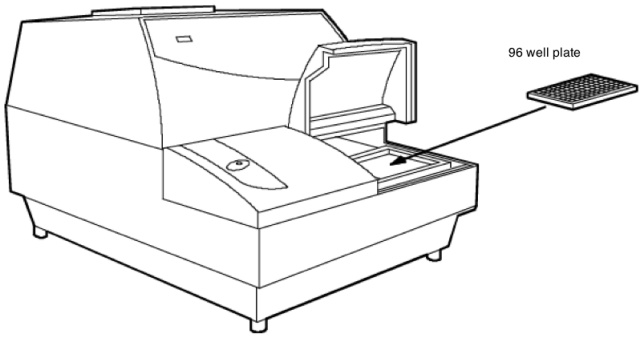

Figure 3–1: Schematic graph of the luminometer used. The samples of different concentration of ATP are places in a 96 well plate. The 96 well plate is inserted into the luminometer for measurement.[6]

A luminometer (Wallac 1420, PerkinElmer) is an instrument for quantitative detection of light emission. Figure 3–1 illustrates the general appearance of a luminometer; the arrow points where the sample is inserted. Due to the set up of this luminometer, the sample must be loaded in a clear bottomed 96 well plate. In an ATP assay, there is no external light source, but light is produced by chemical reactions in the sample. The light emitted then passes through a lens and an empty position in the emission filter to a photomultiplier [6]. The photomultiplier detects the incident light and produces an output signal which gets multiplied from 10 times

up to 108 times [60]. Finally, the signal is collected and detected by an external detector.

3.3.2 ATP calibration curve

The commercialized ATP determination kit (A22066) from Molecular Probes offers an assay for quantitative determination of ATP with firefly luciferase and its substrate D-luciferin [58]. Since this kit is convenient to use, we decided to start ATP calibration with this product. In a 96 well plate, 90uL of the reaction buffer(0.5 mM D-luciferin,1.25 g/mL firefly luciferase, 25 mM Tricine buffer, pH 7.8, 5 mM MgSO4,100 μM EDTA and 1 mM DTT, 100 μM sodium azide) from this kit is placed into each well. Next, 50 nM, 100 nM, 300 nM and 500 nM of ATP is pipetted into the corresponding wells. Each concentration is repeated three times. The 96 well plate is then inserted into the luminometer for measurement in room temperature.

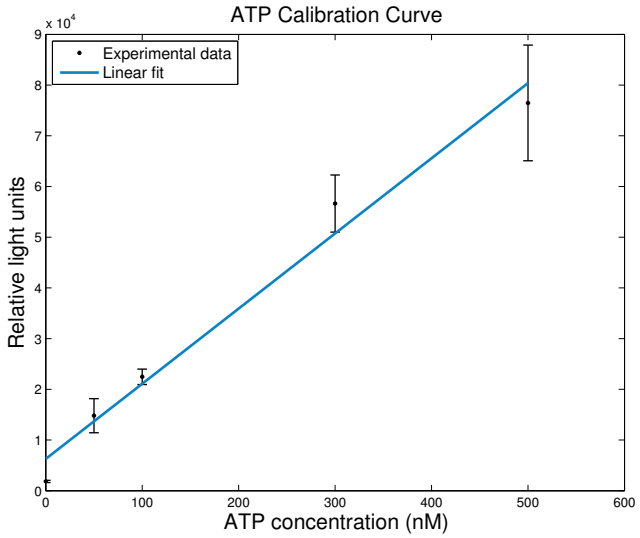

Figure 3–2: Calibration curve of relative light intensity over different concentration of ATP with the prepared buffer from the ATP determination kit. The relationship appears to be linear, with a R^2=0.98

Figure 3–2 illustrates a linear relationship between light intensity and ATP concentration. Each data points are obtained from averaging three trails of the same ATP concentration. The error bars are the standard deviation from the average. This linear relationship confirms that the amount of light produced is directly proportional to the ATP concentration.

In order to use this kit to perform experiment on osteoblasts, the next step is to determine if the reaction buffer can provide an inhabitable environment for the cells.

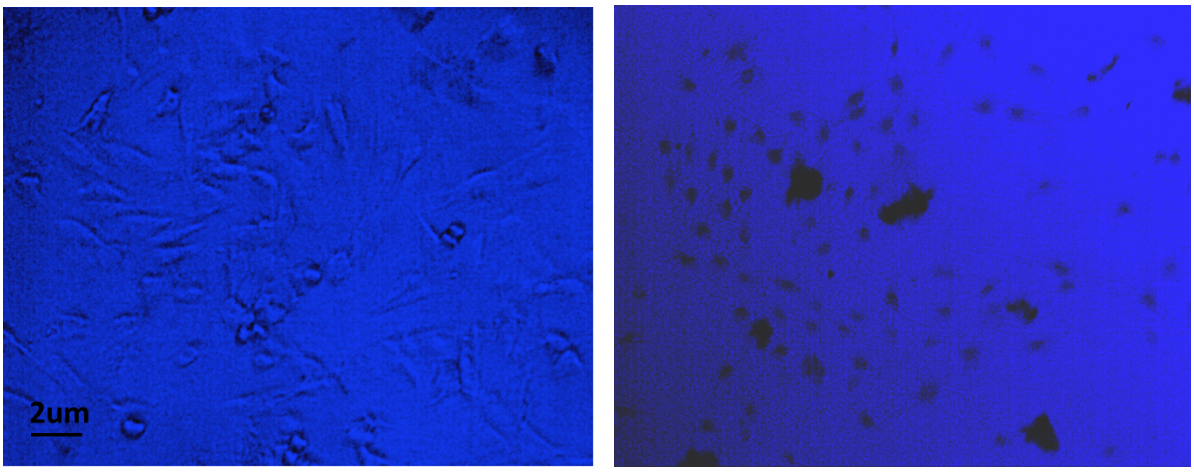

(a) (b)

Figure 3–3: Optical images of two dishes of osteoblasts stained by trypan blue are observed with 10x magnification. Both dishes are incubated for three hours. Trypan blue is added to both dishes before observation. (a) Osteoblasts in DMEM culture media (b) Osteoblasts in reaction buffer from the ATP determination kit. Note that the number of cells stained in dark blue (dead) is much lower when cells are incubated in DMEM culture medium.

Figure 3–3(a) demonstrates a dish of osteoblasts in DMEM culture media; and Figure 3–3(b) shows a second dish of osteoblasts in reaction buffer. Both dishes are incubated in 37^oC and 5% CO_2 for three hours before observation. A vital stain called "trypan blue" is applied to both dishes to selectively color the dead cells blue [61]. Due to the high selectivity of cell membrane, trypan blue compounds are incapable of passing the cell membrane of live cells, leaving them unstained. In Figure 3–3, the cells in DMEM are mostly alive, because they appear transparent, whereas the cells in the reaction buffer are stained blue. Therefore, it can be concluded that the

reaction buffer from the ATP determination kit is toxic to the cells. The toxicity is likely caused by sodium azide in the reaction buffer, a chemical commonly used for bacteria control, which has been proven to be toxic to cells [62].

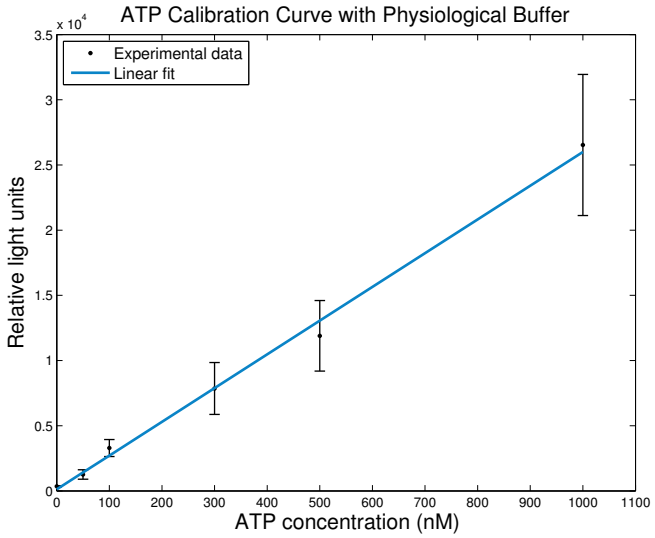

Figure 3–4: Calibration curve of relative light intensity over different concentration of ATP, using physiological buffer. Each ATP concentration is repeated three times. The data points are the average of three measurements.The error bars are the standard deviation of the average. The relationship appears to be linear, with a R^2=0.99.

To avoid toxicity to the cells, the reaction buffer from the ATP determination kit is replaces by a normal physiological buffer (130 mM NaCl;5 mM KCl; 10 mM glucose; 5 mM $MgCl_2$; 1mM $CaCl_2$), which provides an optimum environment for osteoblasts.[63] A second ATP calibration experiment is done using this physiological buffer. The calibration result is demonstrated in Figure 3–4. Similar to the

previous calibration curve in Figure 3–2, the light produced with 50nM, 100nM, 300nM, 500nM and 1000nM of ATP are measured. The linear relationship between the amount of light produced and ATP concentration confirms that the firefly luciferase CL assay works properly in physiological buffer, although the signal intensity is lower, compared to that observed with the commercially supplied reaction buffer. Thus, physiological buffer will be used for future experiment.

CHAPTER 4
ATP Detection Following Mechanical Stimulation with AFM

Atomic force microscopy (AFM) has been recognized to be an advanced instrument to investigate the responses of mechanical stimulation on a single cell level [24] [25]. It is of interest to image ATP release upon mechanical stimulation of osteoblasts. Thus, the goal of this chapter is to investigate whether ATP is released from mechanical stimulation if a single osteoblast. Here, we will first introduce the major principle, components and imaging techniques of AFM. Next, we will describe the standard calibration of ATP using the firefly luciferase chemiluminescence method performed using this setup. Finally, we will show preliminary results on ATP imaging upon mechanical stimulation of osteoblasts.

4.1 Instrumentation

4.1.1 Overview of AFM setup

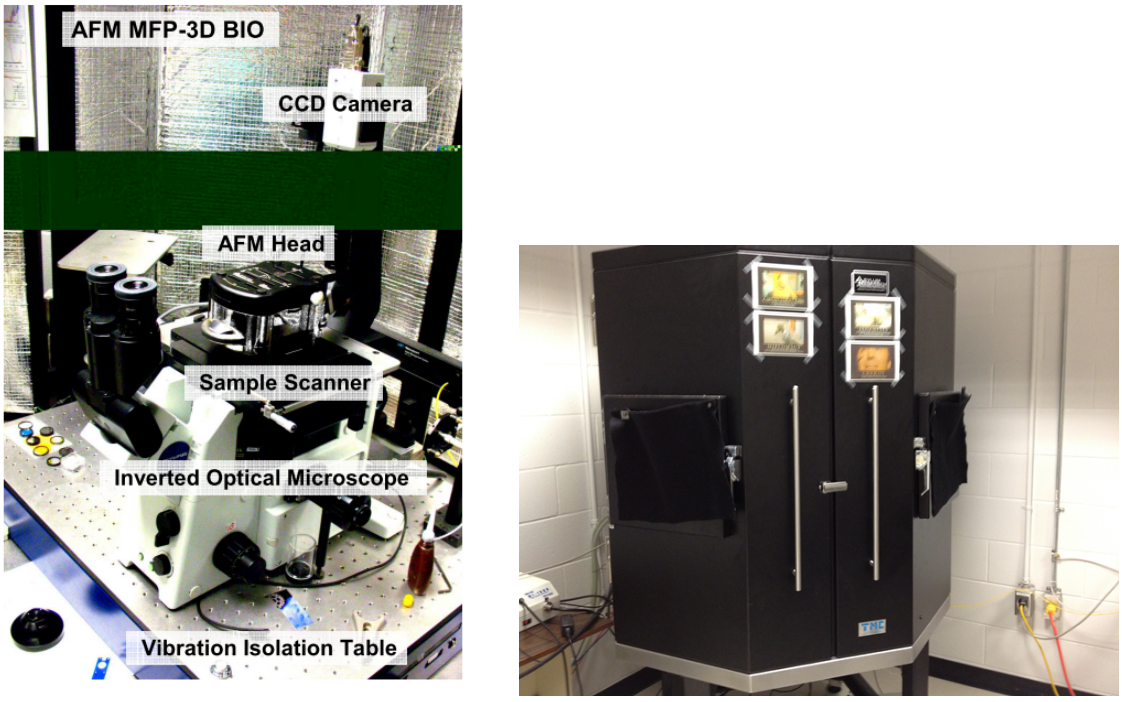

(a) (b)

Figure 4–1: MFP-3D BIO setup.(a) This image is taken from the thesis of Monserratt Lopez's thesis [1]. The image shows the components of the microscope. It is a combination of AFM and inverted optical microscope. The apparatus is mounted on an air table to provide vibration cancelation. This setup is used for mechanical stimulation of cells. (b)The entire apparatus is enclosed in a black box, called the acoustic isolation hood. The hood functions to provide noise and thermal isolation.

A simple introduction of the Atomic Force Microscope (AFM) (Asylum MFP-3D BIO) is given in this section. All the experiments in this chapter will be performed

with this apparatus. Figure 4–1(a) demonstrates the components of our apparatus: AFM Head, Charge Coupled Device (CCD)Camera (Olympus), Sample Scanner, inverted optical microscope and a vibration isolation table (TS300 from Table Stable).

The key component of this apparatus is the AFM head, which modulates the interaction between the cantilever tip and the sample via the movement of z-piezo. The piezoelectric scanner scans the cantilever tip in both X and Y directions to image the sample. During scanning, the laser beam is reflected off the cantilever and detected via a photodiode to monitor the deflection of cantilever. Meanwhile, the feedback signal is sent to the controller to move the scanner in Z direction, providing accurate force and topography measurements.

The component which makes this setup highly suitable for imaging biological samples is combination of AFM with an inverted optical microscope. This combination allows local illumination and detection at the bottom of the sample while applying force spectroscopy simultaneously. Also, the acoustic noise isolation hood is crucial for our experiment, to minimize external light source from entering the chemical reaction of the firefly luciferase assay.

4.1.2 AFM techniques

Next, the interaction mechanism between the AFM tip and the sample will be discussed. There are two commonly used imaging modes: contact mode and tapping mode. The choice of imaging modes is determined by the sample property and the cantilever used. In contact mode, the tip of the cantilever is in direct contact with

the sample, whereas in tapping mode, the cantilever remains at a constant height from the sample while oscillating near its resonant frequency.

Tapping mode

Tapping mode is an important advance in AFM. In tapping mode, the cantilever vibrates at its resonance frequency driven by an external driving force with constant amplitude. Upon approaching the sample, the tip lightly touches or taps the sample surface, resulting in a detectable change in oscillation amplitude [64]. When the tip encounters a fill on the surface, the oscillation amplitude decreases because the cantilever has less room the oscillate. Conversely, passing through a depression on the sample surface causes the oscillation amplitude to increase. These changes in oscillation amplitude are measured by the detector to provide input to the MFP-3D controller. The digital feedback loop adjusts the tip-sample separation to maintain a constant oscillation amplitude and thus tracks the surface topography.

One of the advantages of this image mode is preventing disruption or drag of the sample, especially useful for biological soft samples that are fragile. Also, when imaging under liquid, tapping mode can reduce the high adhesion force due to water film on samples under ambient conditions [65]. Therefore, tapping mode is widely used in obtaining the topographic image of biological samples.

Contact mode

Contact mode is the first mode developed on the AFM, where the tip scans the sample in close contact with the surface [66]. The deflection of the cantilever, resulting from the mechanical contact between the sample and the tip, is kept constant [67]. During scanning of the sample, when the measured deflection is different from the desired value, the feedback amplifier applies a voltage to the piezo to change the position of the cantilever, in order to restore the set value of deflection. The deflected laser position in the z-direction is recorded. The force applied to the sample is easily quantified with this mode. The deflection of the cantilever is proportional to the force acting on the tip, according to Hooke's law:

$$F = -k \times \Delta x \tag{4.1}$$

where Δ x is the deflection of the cantilever and k is the spring constant of the tip.

Compare to tapping mode, contact mode has an obvious disadvantage for sample scanning. The presence of a strong lateral force derived from the scanning motion may produce irreversible damage of the sample.

In our experiment, the response of mechanical stimulation of osteoblasts is measured by force indentation with AFM. Both contact and tapping mode can perform indentation measurement. However, since the force applied is easily quantified by Force-Distance curves in contact mode, we will use contact mode for the following experiments.

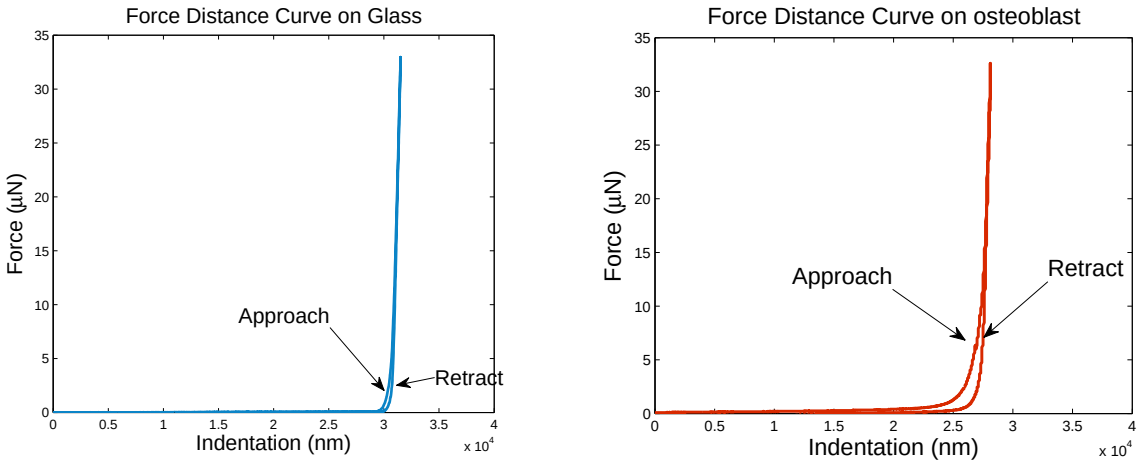

(a) (b)

Figure 4–2: Using a cantilever tip of spring constant (39±2)N/m, Force-Distance curves are plotted for a hard surface (a) glass bottomed coverslip and a biological sample (b)an osteoblast in liquid. The approach and retraction part of the curve are indicated by black arrows.

Figure 4–2 demonstrated the Force-Distance curves of both a hard surface and a soft sample. For a glass surface, the approach curve and the retraction curve are very similar, since the is little hysteresis due to a lack of adhesion. However, when the sample is soft, as for most biological samples, the force applied creates a surface deformation on the sample, which causes a more gradual increase of the force. As shown in Figure 4–2(b), the rise of the approach curve is less steep, compare to the hard glass surface. During retraction of the cantilever, the biological samples shown more adhesion and therefore, there is more hysteresis between the approach and the retraction curves for the osteoblast.

4.2 ATP calibration on AFM setup

4.2.1 Modification to the Setup

The first attempt to image ATP directly is realized with the setup in Figure 4–3.

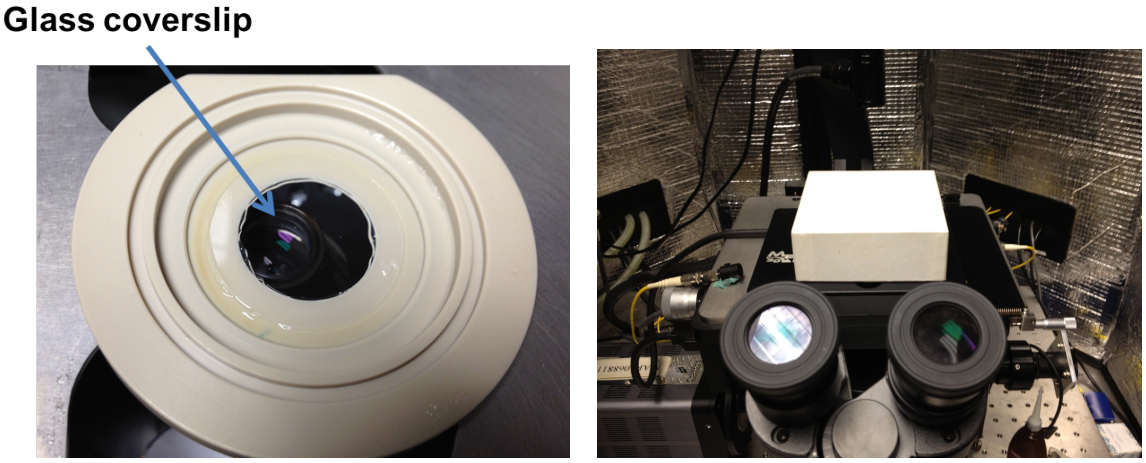

(a) (b)

Figure 4–3: (a)An image of a glass coverslip glued to the sample holder. The reaction mixture will be added to the coverslip (b)This is the original set-up where the sample holder is inside the white box. The box prevents external light from entering the sample and interfering with the luciferin/luciferase reaction.

A 25 mm glass coverslip (Deckglaser Cover Glasses) is placed inside the sample holder, illustrated in Figure 4–3(a). 15 μl of reaction mixture consist of 2 mM of D-luciferin and 2 mg/ml of luciferase in physiological buffer is added to the glass coverslip. The detection of the faint light produced by the luciferin/luciferase chemical reaction is challenging. In order to maximize the light detection, the external light sources need to be eliminated. Thus, a white box is placed on the sample holder to

minimize the effect of external light, shown in Figure 4–3(b). The acoustic isolation hood (black box) of the AFM is also closed. 60 frames of images with 1s exposure time and 95 ms delay between frames are taken with a CCD camera, where 500 μM of ATP is added at frame 10. However, this experiment was not successful due to the weak signal to noise ratio, making it difficult to extract the signal from the light produced via the reaction. A possible reason of this failure is that during imaging, when ATP is added via a pipette, both the external black case of the AFM and the white box need to be opened. This can cause the external light to enter the sample and influence the reaction.

To prevent the external light source from entering the reaction, the setup is changed to keep the acoustic isolation hood closed at all times during the experiment.

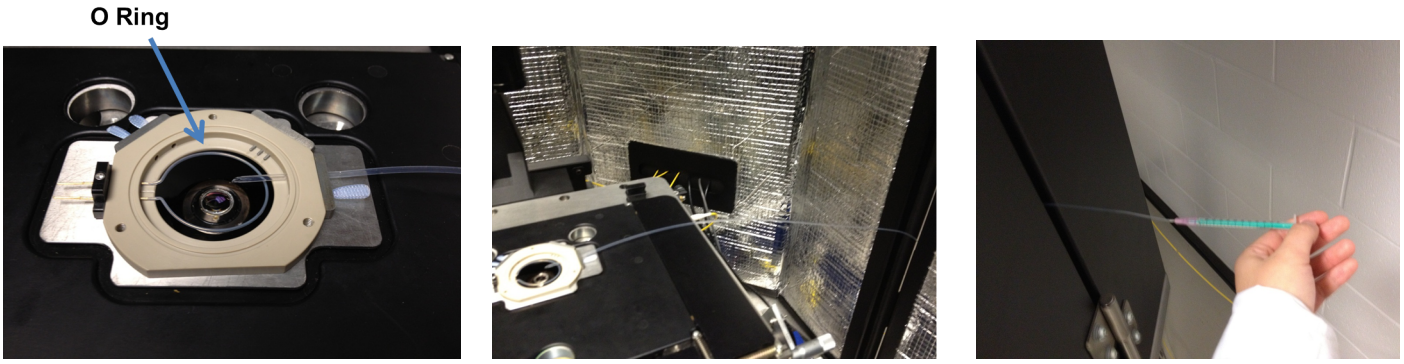

(a) (b) (c)

Figure 4–4: (a)A picture of the sample holder. The tube is inserted to approximately the middle of the imaging field. (b)The tube is extended to the outside of the AFM isolation box. (c) A 1ml syringe is attached at the end of the tube. ATP solution are injected from the syringe to the sample.

A piece of polymer tubing (Upchurch Scientific) is inserted via an opening on the side of the sample holder, shown in Figure 4–4(a). Before the experiment, 15 μl of luciferin/luciferase reaction mixture is injected into the O-ring chamber on the glass coverslip. 500 μM of ATP solution is then loaded inside the tubing. This tubing is extended to the outside of the acoustic isolation hood, with a 1ml syringe (Henke Sass Wolf GmbH) attached at the other end. With this setup, the acoustic isolation hood of the AFM remains closed throughout the experiment and ATP is injected by the syringe.

4.2.2 ATP calibration with AFM

The light generated by the chemical reaction is recorded by a CCD camera for a total of 100 images. The exposure time is 1s and the delay between consecutive images is 95ms.

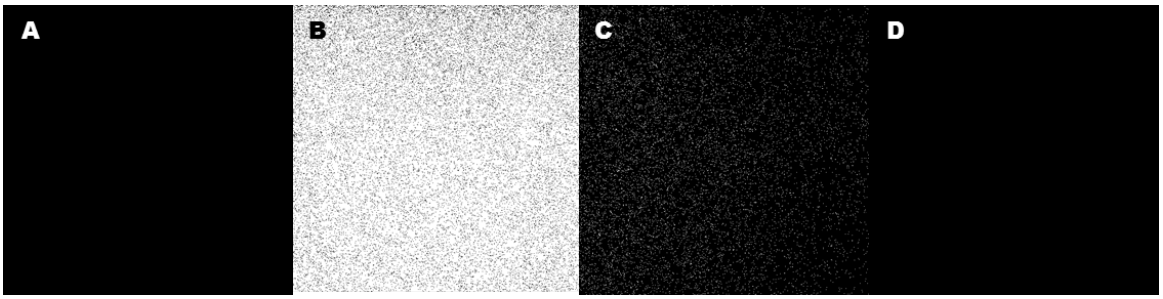

Figure 4–5: Standard ATP detection. 500 μM of ATP was injected with a syringe into a mixture of D-luciferin and firefly luciferase on coverslips. (A)Image taken at t = 0 ms, no ATP was added. (B)Firefly luciferase detection image: intense chemiluminescence light is produced when ATP is added to 2 mg/ml firely luciferase and 2mM D-luciferin at t = 1100 ms. (C)Firefly luciferase detection image taken at t = 4000 ms:the intensity of chemiluminescence light decreases. (D)Firefly luciferase detection image taken at t = 10000 ms: the intensity of chemiluminescence light significantly decreases.

The first 10 images are taken without injection of ATP as background reference. 500 μM of ATP is injected with a syringe at image 11. Figure 4–5 (B) demonstrated a large amount of chemiluminescence light produced upon the addition of ATP. The light intensity then decreases with time.

The chemiluminescence intensity is plotted against time in Figure 4–6. When ATP is added at approximately 1100ms to the mixture of D-luciferin and firefly luciferase in the o-ring chamber, a sharp increase in the light intensity appears within 1-2 s, followed by a decrease in light intensity gradually over time to reach a plateau.

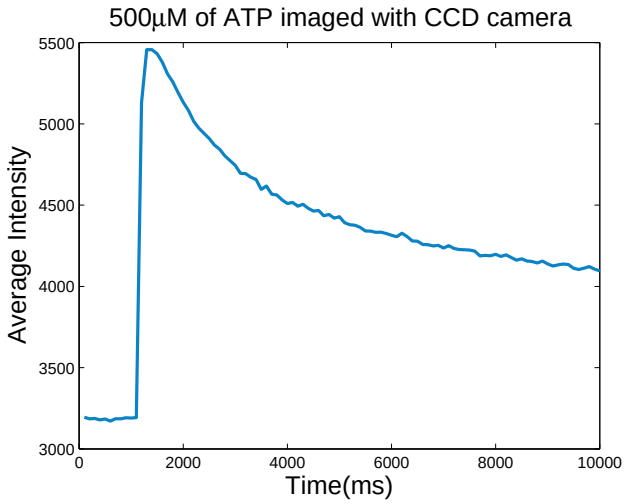

Figure 4–6: The average light intensity is plotted against time of the addition of 500 μM ATP to a 2 mM D-luciferin and 2 mg/ml firefly luciferase reaction mixture.

Next, the standard calibration is performed by injecting 5 μM, 50 μM, 100 μM and 500 μM of ATP into the luciferin/luciferase reaction mixture. Due to the limited availability of the enzyme, firefly luciferase, only these four concentrations are tested.

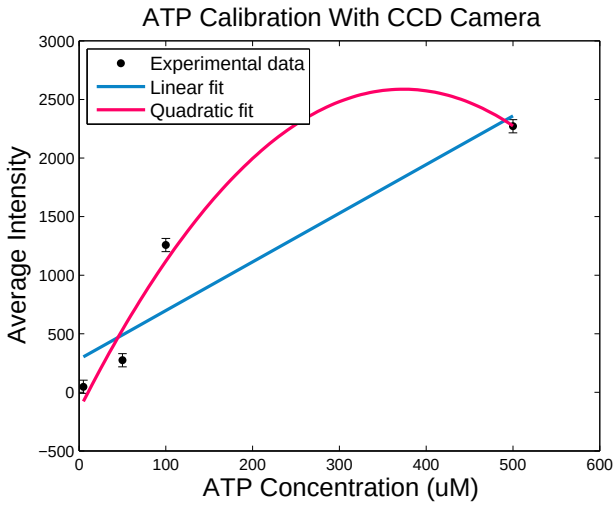

Figure 4–7: This plot shows a standard calibration curve. The amplitude of light intensity is plotted against ATP concentration. The average background intensity calculated by averaging the first 10 images. The error bars are obtained from taking the square root of the average background intensity (shotnoise). The blue curve represents the linear fit of the data with $R^2 = 0.86$ and the read curve represents the quadratic fit with $R^2 = 0.97$.

In Figure 4–7, the amplitude of the light intensity is plotted against ATP concentration. These four data points are fitted both linearly and quadratically. Surprisingly, compare the $R^2 = 0.86$ for linear fit and the $R^2 = 0.97$ for the quadratic fit, one can conclude that the light intensity appears to have a non-linear relationship with the increase of ATP concentration. A possible explanation could be that some of the enzyme may be absorbed to the coverslip surface with compromised light production efficiency [32], however, more data points with various ATP concentrations need to be generated to be conclusive.

4.3 Mechanical Stimulation of Osteoblast with AFM

To investigate if ATP is the intercellular signal mediator upon mechanical stimulation, cultured C2C12 cells (osteoblasts) on a 25 mm coverslip are washed with 1ml of physiological buffer ((130 mM NaCl, 4 mM KCl, 10 mM glucose, 1 mM $MgCl_2$, 1 mM $CaCl_2$ and 20 mM HEPES.) and placed on the o-ring of the sample holder. 200 μl of the luciferin/luciferase reaction mixture is added on top of the cells to maintain their viability. The light produced in response of ATP release is captured via the inverted optical microscope with the 40x objective. Videos of the experiment is acquired using a CCD camera, where the exposure time is 1s and the delay between consecutive images is 95 ms. The first 7 images are taken as reference. The tip approaches the cell at approximately the 8th image.

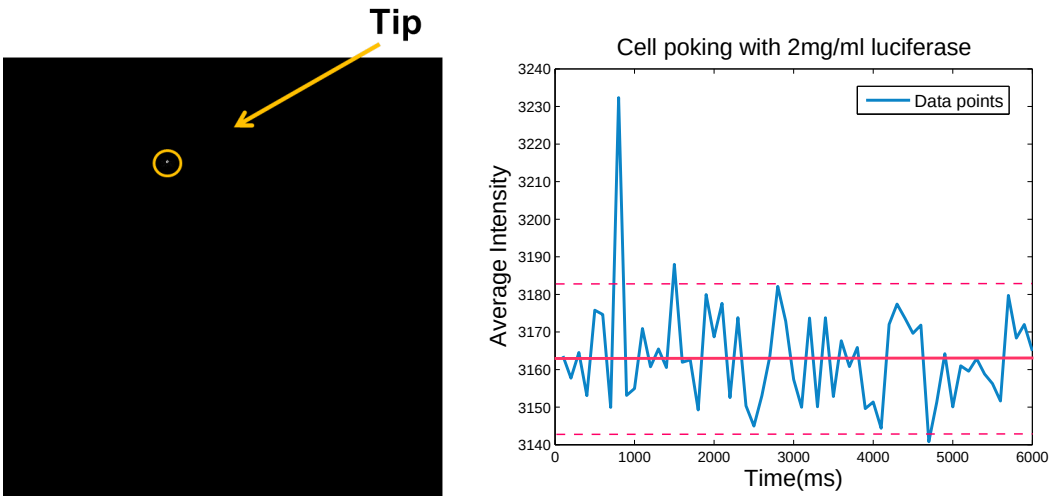

(a) (b)

Figure 4–8: (a) An osteoblast is mechanically stimulated via a cantilever tip of spring constant (39±2)N/m. The yellow circle indicates the position of the tip. (b) Average light intensity against imaging time are plotted. The average intensity peaks at approximately 8th frames. The solid pink line indicates the average background noise and the dotted lines are the root mean squared of the noise level.

A single osteoblast is mechanically stimulated via a (39±2) N/m cantilever tip with the approaching speed of 2 μm/s, as shown in Figure 4–8(a). The average light intensity profile is analyzed via ImageJ software and plotted against imaging time. Figure 4–8(b) illustrates a peak in the average intensity at approximately 8th image. Since the peak value is larger than the root mean squared of the background noise level, the peak signal is statistically significant. One drawback of this experiment if that it is challenging to determine the exact position of the cantilever tip, due to the

fact that the imaging field is completely dark. Therefore, further experiments need to be performed to confirm this result.

4.4 Future directions

The information of mechanical stimulation can be provided by performing a Force-Distance (FD) curve on top of an osteoblast. Figure 4–9(a) demonstrates the FD curve of the mechanically stimulated osteoblast. The smoothness of the approach curve implies that the cell membrane is deformed.

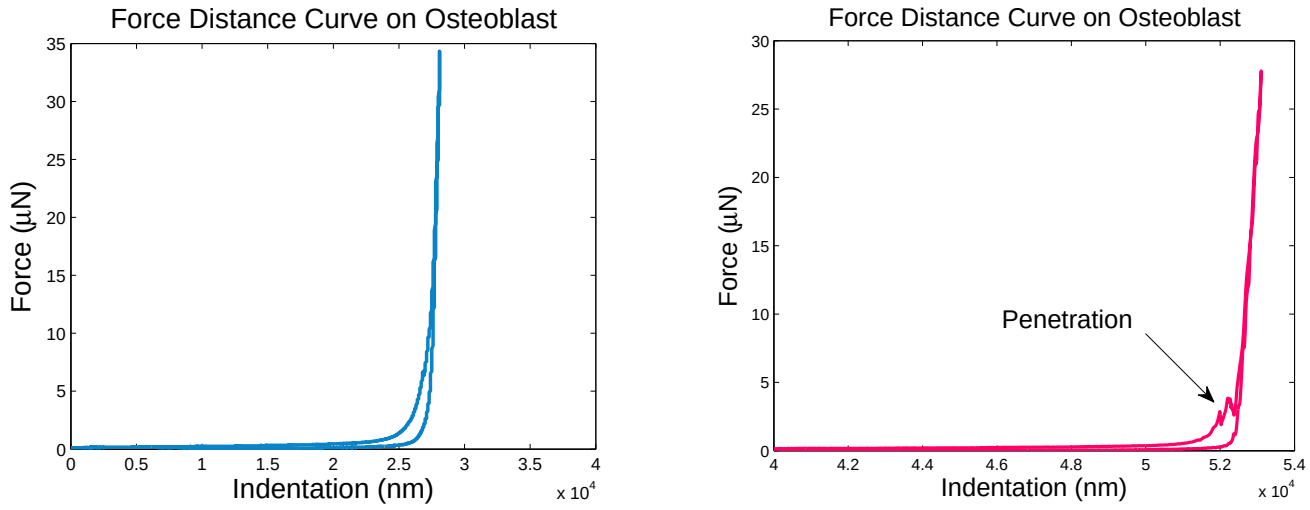

(a) (b)

Figure 4–9: (a) Using a cantilever tip of spring constant (39±2) N/m, Force-Distance curve is plotted for the indentation of an osteoblast. The local indentation has deformed the cell membrane. (b) Force-Distance curve of cell indentation is plotted with a cantilever tip of (41±2) N/m. The small bump on the curve indicates the cell membrane is penetrated.

In order to increase the ATP released from the cell, a stiff cantilever (k=41± 2 N/m)is used to damage the cell membrane. The FD curve taken over an osteoblast is plotted in Figure 4–9(b). The small increase on the approaching side indicates membrane rupture. Theoretically, larger amount of ATP would be released when the cell membrane is damaged. Therefore, the next step of the experiment is to investigate if ATP is released from the cell, when the cell membrane is ruptured.

CHAPTER 5
Conclusion

Mechanical loading is crucial in modulating the physiology and architecture of bone tissue. Extracellular ATP was previously shown to function as a mediator of mechanically induced signaling [33]. To investigate the mechanisms of ATP signaling, propagation and release, both mathematical modeling and direct experimental approaches were used. ATP acts on osteoblasts through P2X, ligand gated ion channels and P2Y, G-protein coupled receptors. The ATP dose response for each P2 receptor was described using the Hill Equation. It was found that P2 receptors are activated in a wide range of ATP concentration from 1×10^{-9} M to 1×10^{-2} M. Through collaboration with Dr. Dixon's group from University of Western Ontario, we received experimental measurements on the calcium level increase in osteoblasts after the application of various ATP concentrations. Fitting the P2 receptors model to these experimental data allowed us to determine the role of individual receptors. We have shown that: 1) the initial increase in the amount of calcium is likely caused by $P2Y_2$ receptor; 2) $P2X_7$ receptor is responsible for the increase in both calcium amount and response duration at millimolar concentrations of ATP; 3) the other receptors likely have an inhibitory effect on the calcium response. Next, we used mathematical modeling and simulations to study the process of ATP degradation via extracellular nucleotidases and the diffusion of resulting ATP, ADP and AMP through the medium. Upon mechanical stimulation, ATP is released from the source

cell. From this model, one can predict that the concentration of ATP, ADP and AMP decreases with time and distance from the source. Interestingly, due to ATP degradation, the main propagating mediator may change from ATP to ADP to AMP over distance. Finally, we attempted to directly measure ATP released from the mechanically stimulated cells. The firefly luciferase assay was successfully utilized to detect ATP. Mechanical stimulation of a single osteoblast was performed by local indentation with the AFM cantilever tip. Although the preliminary experimental results did not fully demonstrate the real time detection of ATP release from a single osteoblast, the potential technical problems were identified and future experimental studies are proposed. Taken together, the studies described in this thesis provide new insights into the mechanisms of mechanically induced intercellular signaling by ATP.

References

[1] Lopez Gabriela Monserratt. Applying a commercial atomic force microscope for scanning near-field optical microscopy techniques and investigation of cell-cell signaling. *Dessertation*, 2009.

[2] Osama Mohamed Maria. Intercellular propagation of singal induced by mechanical stimulation of a single bone cell. *Dessertation*, 2009.

[3] http://www.celanphy.science.ru.nl/bruce20web/flash20movies.htm.

[4] R J Evans et al. Pharmacological characterization of heterologously expressed atp-gated cation channels (p2x purinoceptors). *Molecular Pharmacology*, 48:2178–2183, 1995.

[5] Ellen L.gordon et al. The hydrolysis of extracellular adenine nucleotides by arterial smooth mucle cells. *The Joural of Biological Chemistry*, 264:18986–18992, 1989.

[6] Perkin Elmer. Instrument manual. *Perkin Elmer*, 2003.

[7] Standring S. *Musculoskeletal system.* Elsevier, New York, USA, 2004.

[8] Bart Clarke et al. Normal bone anatomy and physiology. *Clinical Journal of the American Society of Nephrology*, 3:5131–5139, 2008.

[9] John A.Kanis et al. The diagnosis of osteoporosis. *Journal of bone and mineral research*, 9:1137–1141, 1994.

[10] Seicho Makihira et al. Impact o the microgravity environment in a 3-dimensional clinostat on osteoblast and osteoclast-like cells. *Cell Biology International*, 32:1176–1181, 2008.

[11] Russell T. Turner. Invited review: What do we know about the effect of apce flight on bone? *Journal of Applied Physiology*, 89:840–847, 2000.

[12] A.Glucksmann. Studies on bone mechanics in vitro. the rold of tension and pressure in chondrogenesis. *The Anatomical Record*, 73:39–55, 1939.

[13] Rodan G.A. Bourret, L.A. The role of calcium in the inhibition of camp accumulation in epiphyseal cartilage cells exposed to physiological pressure. *Journal of Cell Physiology.*, 88:353–361, 1976.

[14] Thomas D.Brown. Techniques for mechanical stimulation of cells in vitro: a review. *Journal of biomechanics*, 33:3–14, 2000.

[15] Hiroyuki Ozawa et al. Continuously applied compressive pressure induceds bone resorption by a mechanism involving prostaglandin e2 synthesis. *Journal of Cell Physiology.*, 144:224–228, 2005.

[16] Leung et al. A new in vitro system for studying cell response to mechanical stimulation. *Experimental Cell Research.*, 109:285–298, 1977.

[17] C et al. Neidlinger-Wilke. Dynamic stretching of human osteoblasts: an experimental model for in vitro simulation of fracture gap micromotion. *Journal of Orthopaedic Research.*, 12:70–78, 1994.

[18] S. et al. Hasegawa. Mechanical stretching increases the number of cultured bone cells synthesizing dna and alters their pattern of protein synthesis. *Calcified Tissue International*, 37:431–436, 1985.

[19] Schaffer et al. Device for the application of a dynamically bizxially uniform and isotropic strain to a flexible cell culture membrane. *Journal of Orthopaedic Research*, 12:709–719, 1994.

[20] C.F. Dewey. Effects of fuild flow on living vascular cells. *Journal of Biomechanical Engineering*, 106:31–35, 1984.

[21] Nerem R.M. Levesque, M.J. The elongation and orientation of cultured endothelial cells in response to shear stress. *Journal of Biomechanical Engineering*, 107:341–347, 1985.

[22] S.L. Xia and J. Ferrier. Propagation of a calcium pulse between osteoblastic cells. *Biochemical and biophysical research communications*, 186:1212–1219, 1992.

[23] et al. Kirber, M.T. Multiple pathways responsible for the stretch-induced increase in ca2+ concentration in toad stomach smooth muscle cells. *Journal of Physiology*, 524:3–7, 2000.

[24] et al. Charras, G.T. Estimating the sensitivity of mechanosensitive ion channels to membrane strain and tension. *Biophysical Journal*, 84:2870–2874, 2004.

[25] et al. Guo, X.E. Intracellular calcium waves in bone cell networks under single cell nanoindentation. *Mol Cell Biomech*, 3:95–107, 2006.

[26] J. L. Alonso and W. H. Goldmann. Feeling the forces: atmoic force microscopy in cell biology. *Life Sciences.*, 72:2553–2560, 2003.

[27] Hamid Ladjal et al. Atomic force microscopy-based single cell indentation: Experimentation and finite element simulation. *IEEE/RSJ International Conference on Intelligent Robots and Systems.*, 2009.

[28] et al. Chen, N.X. ca^{2+} regulates fluid shear-induced cytoskeletal reorganization and gene expression in osteoblasts. *Am J Physiol Cell Physiol*, 275, 2000.

[29] et al. Hung, C.T. Real-time calcium response of cultured bone cells to fluid flow. *Clin Orthop Relat Res*, 313, 1995.

[30] Molecular Probes. Fura and indo ratiometric calcium indicators. *Molecular Probes Invitrogen Detection Techologies*, 2011.

[31] Purves et al. Neuroscience. *4th ed*, Sinauer Associates:156–7, 2008.

[32] Yun Zhang. Real time imaging of live cell atp leaking or release events by chemiluminescence microscopy. *Dessertation*, 2008.

[33] G. Burnstock. Purinergic nerves. *Pharmacol. Rev.*, 24:509–581, 1972.

[34] A. Zsembery E.M. Schwiebert. Extracellular atp as a signaling mole- cule for epithelial cells. *Biochim. Biophys. Acta*, 24:7–32, 2003.

[35] J. Linden R.E. Bucheimer. Purinergic regulation of epithelial transport. *J. Physiol.*, 555:311–321, 2004.

[36] C. Gachet. Regulation of platelet functions by p2 receptors. *Annual Rev. Pharmacol. Toxicol.*, 46:277–300, 2006.

[37] G.T.Charras and M.A.Horton l. Single cell mechanotransduction and its modulation analyzed by atomic force microscope indentation. *Biophysics Journal*, 82(6):2970–2981, 2002.

[38] S.J.Dixon et al. Activity-dependent development of p2x7 current and ca^{2+} entry in rabbit osteoclasts. *J.Biol Chem l*, 276(42):39107–39114, 2001.

[39] Gennady G. Yegutkin et al. The detection of micromolar pericellular atp pool on lymphocyte surface by using lymphoid ecto-adenylate kinase as intrinsic atp sensor. *Mol. Biol. Cell*, 17:3378–3385, 2006.

[40] Herbert Zimmermann. Extracellular metabolism of atp and other nucleotides. *NaunymSchmiedeberg's Arch Pharmacoll*, 362:299–309, 2000.

[41] Bruce C.Veit et al. Increased adenosine deaminase activity and a shift from ada-dependent to ada-independent phases during t-cell activation: A paradox. *JNCl*, 72(5), 1984.

[42] T K Harden et al. Signalling and pharmacological properties of the p2y14 receptor. *Acta Physiol*, 199:149–160, 2010.

[43] Miguel Garcia guzman et al. Characterization of recombinant human p2x4 receptor reveals pharmacoloical difference to the rat homologue. *Molecular Pharmacology*, 51:109–118, 1997.

[44] R. G. D. Steel and J. H. Torrie. *Principles and Procedures of Statistics*. McGraw-Hill, New York, USA, 1960.

[45] Shinghua Ding et al. Single channel properties of p2x2 purinocepters. *JGP vol.*, 113:5695–720, 1999.

[46] C. Lewis S. Neidhart et al. Coexpression of p2x2 and p2x3 receptor subunits can account for atp-gated currents in sensory neurons. *Nature*, 377:432 – 435, 1995.

[47] William R. Haines et al. Properties of the novel atp-gated ionotropic receptor composed of the p2x1 and p2x5 isoforms. *Molecular Pharmacology*, 56:720–727, 1999.

[48] Soto F et al. Cloning and tissue distribution of a novel p2x receptor from rat brain. *Biochem Biophys Res Commun*, 223:456–460, 1996.

[49] A. Surprenant et al. The cytolytic p2z receptor for extracellular atp identified as a p2x receptor (p2x7). *Science*, 272:735–738, 1996.

[50] Catherine Lon et al. The p2y1 receptor is an adp receptor antagonized by atp and expressed in platelets and megakaryoblastic cells. *FEBS Letter*, 403:26–30, 1997.

[51] Robert A. Nicholas et al. Uridine nucleotide selectivity of three phospholipase c activating p2 receptors: Identification of a udp-selective, a utp-selective, and an atp- and utp-specific receptor. *Molecular pharmacology*, 50:224–229, 1996.

[52] Pamela J. White et al. Characterization of a ca response to both utp and atp at human p2y11 receptors: Evidence for agonist-specific signaling. *Mol Pharmacol*, 63:1356–1363, 2003.

[53] Steven J. Ennion et al. Identification of the p2y12 receptor in nucleotide inhibition of exocytosis from bovine chromaffin cells. *Mol Pharmacol*, 66:601–611, 2004.

[54] T K Harden et al. Signaling and pharmacological properties of the p2y14 receptor. *Acta Physiol*, 199:149–160, 2010.

[55] James Herod Ronal W.Shonkwiler. *Mathematical Biology*. Springer, New York, USA, 2000.

[56] Marko Vendelin and Rikke Birkedal. Anisotropic diffusion of fluorescently labeled atp in rat cardiomyocytes determined by raster image correlation spectroscopy. *American Journal of Phyiology Cell Physiology*, 295:C1302–C1315, 2008.

[57] Yun Zhang et al. Imaging localized astrocyte atp release with firefly luciferase beads attached to the cell surface. *Anal.Chem*, 80:9316–9325, 2008.

[58] Molecular Probes. Atp determination kit (a22066). *Invitrogen detection technologies*, 2005.

[59] P.E. Stanley et al. *ATP luminescence : rapid methods in microbiology*. Blackwell Scientific Publications, 1989.

[60] Hamamatsu. *Photomultiplier tubes basics and applications*. Hamamatsu Photonics K.K, 2006.

[61] H. M. Shapiro. *Practical Flow Cytometry*. Jhn Wiley and Sons, New York, 1988.

[62] Lamm SH Chang S. Human health effects of sodium azide exposure: a literature review and analysis. *Int J Toxicol*, 22(3):175–86, 2003.

[63] Naomi Kemeny-Suss et al. Alendronate affects calcium dynamics in cardiomyocytes in vitro. *Vascular Pharmacology*, VPH:05789, 2009.

[64] Constant A.J.Putman et al. Tapping mode atomic force microscopy in liquid. *Applied Physics Letter*, 64:2454–2456, 1994.

[65] A.L.Weisenhorn et al. Forces in atomic force microscopy in air and water. *Applied Physics Letter*, 54:2651, 1989.

[66] G. Binnig et al. Atomic force microscopy. *Physical Review Letter*, 56:930–933, 1986.

[67] F. Moreno-Herrero et al. Atomic force microscopy contact, tapping, and jumping modes for imaging biological samples in liquids. *Physical Review E*, 69:031915, 2004.